NASA TechBriefs

National Aeronautics and
Space Administration

Electronic Components and Circuits

Electronic Systems

Physical Sciences

Materials

Computer Programs

Mechanics

Machinery

Fabrication Technology

Mathematics and Information Sciences

Life Sciences

INTRODUCTION

Tech Briefs are short announcements of innovations originating from research and development activities of the National Aeronautics and Space Administration. They emphasize information considered likely to be transferable across industrial, regional, or disciplinary lines and are issued to encourage commercial application.

Availability of NASA Tech Briefs and TSPs

Requests for individual Tech Briefs or f Technical Support Packages (TSPs) announced herein should be addressed to

National Technology Transfer Center
Telephone No. **(800) 678-6882** or via World Wide Web at **www2.nttc.edu/leads/**

Please reference the control numbers appearing at the end of each Tech Brief. Information on NASA's Commercial Technology Team, its documents, and services is also available at the same facility or on the World Wide Web at **www.nctn.hq.nasa.gov**.

Commercial Technology Offices and Patent Counsels are located at NASA field centers to provide technology-transfer access to industrial users. Inquiries can be made by contacting NASA field centers and program offices listed below.

NASA Field Centers and Program Offices

Ames Research Center
Carolina Blake
(650) 604-0693 or
cblake@mail.arc.nasa.gov

Dryden Flight Research Center
Lee Duke
(805) 258-3802 or
lee.duke@dfrc.nasa.gov

Goddard Space Flight Center
George Alcorn
(301) 286-5810 or
galcorn@gsfc.nasa.gov

Jet Propulsion Laboratory
Merle McKenzie
(818) 354-2577 or
merle.mckenzie@ccmail.jpl.nasa.gov

Johnson Space Center
Hank Davis
(281) 483-0474 or
hdavis@gp101.jsc.nasa.gov

John F. Kennedy Space Center
Gale Allen
(407) 867-6526 or
galeallen-1@ksc.nasa.gov

Langley Research Center
Dr. Joseph S. Heyman
(804) 864-6006 or
j.s.heyman@larc.nasa.gov

Glenn Research Center
Larry Viterna
(216) 433-3484 or
cto@lerc.nasa.gov

George C. Marshall Space Flight Center
Sally Little
(256) 544-4266 or
sally.little@msfc.nasa.gov

John C. Stennis Space Center
Kirk Sharp
(228) 688-1929 or
ksharp@ssc.nasa.gov

NASA Program Offices
At NASA Headquarters there are seven major program offices that develop and oversee technology projects of potential interest to industry:

Carl Ray
Small Business Innovation Research Program (SBIR) & Small Business Technology Transfer Program (STTR)
(202) 358-4652 or
cray@mail.hq.nasa.gov

Dr. Robert Norwood
Office of Aeronautics and Space Transportation Technology (Code R)
(202) 358-2320 or
rnorwood@mail.hq.nasa.gov

John Mulcahy
Office of Space Flight (Code MP)
(202) 358-1401 or
jmulcahy@mail.hq.nasa.gov

Gerald Johnson
Office of Aeronautics (Code R)
(202) 358-4711 or
g_johnson@aeromail.hq.nasa.gov

Bill Smith
Office of Space Science (Code S)
(202) 358-2473 or
wsmith@sm.ms.ossa.hq.nasa.gov

Roger Crouch
Office of Microgravity Science Applications (Code U)
(202) 358-0689 or
rcrouch@hq.nasa.gov

Granville Paules
Office of Mission to Planet Earth (Code Y)
(202) 358-0706 or
gpaules@mtpe.hq.nasa.gov

NASA TechBriefs

4

Electronic Components and Circuits

Hardware, Techniques, and Processes

High-Power-Density DC-to-DC Power-Converter Modules

Major features include multilayer hybrid packaging and a transformer-coupling feedforward/feedback control scheme.

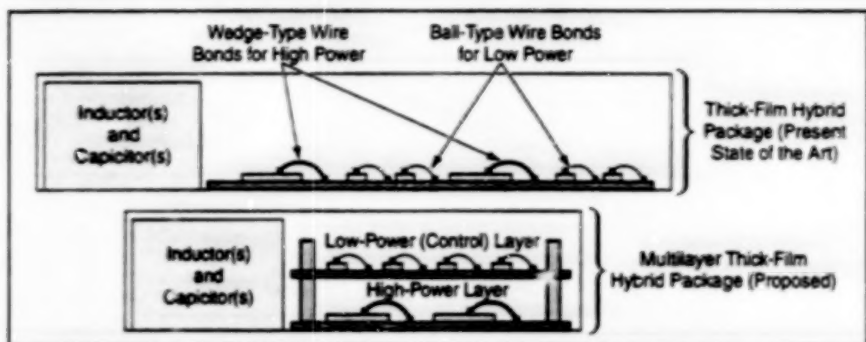*John H. Glenn Research Center,*
Cleveland, Ohio

Figure 1. The **Multilayer Thick-Film Hybrid** approach makes it possible to use package volume more efficiently than does the state-of-the-art single-layer thick-film hybrid approach.
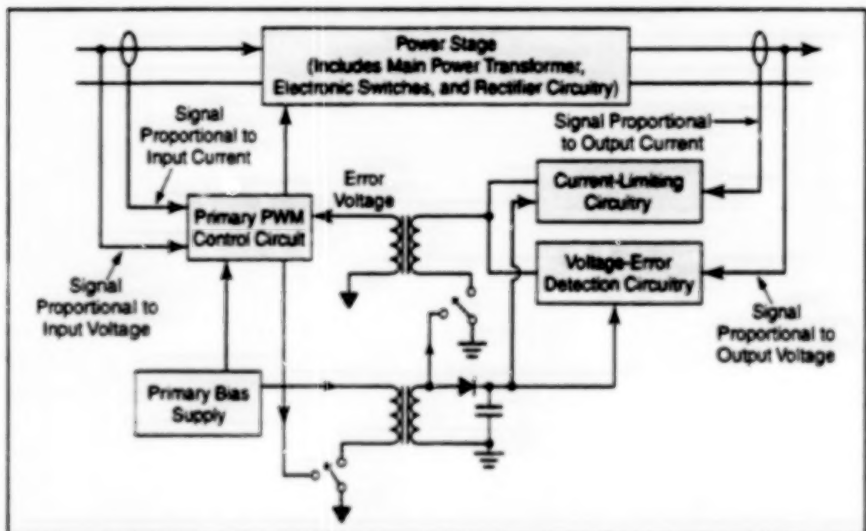

Figure 2. This **Transformer-Coupled Feedforward/Feedback** control scheme offers advantages of greater reliability and functionality, relative to power-converter control schemes based on optocouplers.

Dc-to-dc power-converter modules that operate with input potentials from 60 to 140 V and generate various output potentials up to 15 V are undergoing development. Designed specifically for use aboard planned spacecraft wherein electric power will be supplied at bus potentials from 70 to 120 V, these power-converter modules could also be useful in a variety of terrestrial applications. The fully developed versions of these power-converter modules are expected to operate at power densities about 33 percent greater than those of currently available commercial 28-V-input power-converter modules.

The increase in power density will be achieved by use of multilayer thick-film hybrid packaging conceived expressly for this purpose. This can be explained by reference to Figure 1, which depicts a typical state-of-the-art power converter of single-layer thick-film hybrid design and a proposed electrically equivalent power converter of a two-layer thick-film hybrid design. In addition to large inductors and capacitors for storing energy, there is hybrid circuitry that includes (1) low-power signal-level control devices connected by ball-type wire bonds and (2) high-power devices connected by wedge-type wire bonds. The high-power devices must be mounted with low thermal resistances between themselves and a heat sink; therefore, the high-power devices must be mounted on a substrate in contact with the floor of the converter housing.

The heat-sinking requirement for the low-power devices is less stringent, making it possible to mount these devices on a substrate not in direct contact with the heat sink. Taking advantage of this possibility in the proposed two-layer design, the low-power devices would be placed on a separate substrate. The high-power layer would still be mounted in contact with the heat sink, but the low-power-device layer would be mounted above the high-power layer, so that the floor area occupied by the power-converter circuitry would be less than it is in the single-layer design. Thus, for a given power throughput, the package could be made smaller; in other words, the power density could be larger.

Another notable feature of the developmental power converters is a transformer-coupled feedforward/feedback control scheme (see Figure 2). Heretofore, it has been common practice to implement power-converter control circuitry with optocouplers for electrical isolation between input and output sides. However, optocouplers lack the long-term reliability required for the intended spacecraft application. In the developmental control scheme, pulse-width-modulation (PWM) control of the power supplied to the primary winding of a main power transformer is effected on the input side, while sensing of output current and voltage is effected on the output side (the secondary side of the main power transformer).

Power for the secondary-side control circuitry is provided from the primary side through a pulse transformer (distinct from the main power transformer) excited at the switching frequency. An error signal from the control circuitry on the secondary side is fed back to the control circuitry on the primary side via another pulse transformer. This transformer-coupled feedforward/feedback scheme makes it possible to turn on the secondary-side control circuitry before turning on the main power, thereby making it possible to exert control over the output during startup and during recovery from transient short-circuit conditions.

Optically Transparent Patch Antennas

Antennas on transparent films can be bent to conform to curved supports.
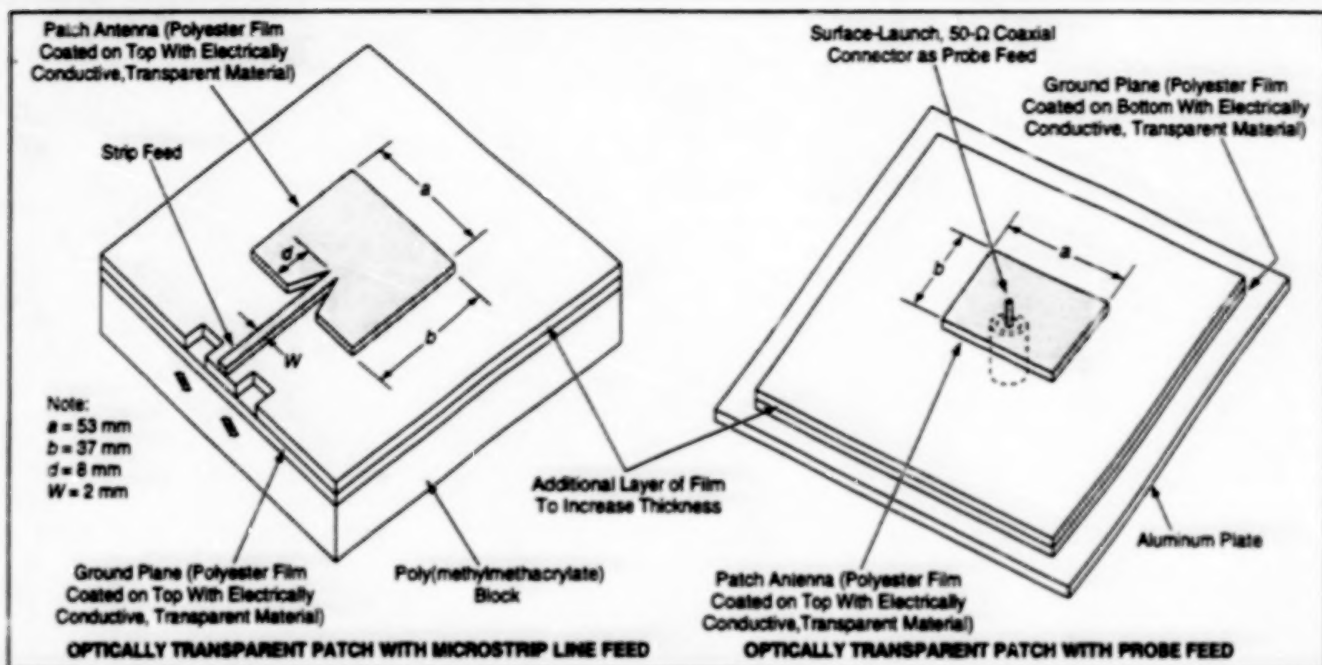
John H. Glenn Research Center, Cleveland, Ohio

Figure 1. **Coated Polyester Films Cut to Required Patterns** can be used to construct optically transparent patch antennas. These are only two examples of the unlimited number of antenna configurations. The poly(methyl methacrylate) block and aluminum plate in these examples are used for mechanical support only; in a typical application, the support would be a window or other transparent object.
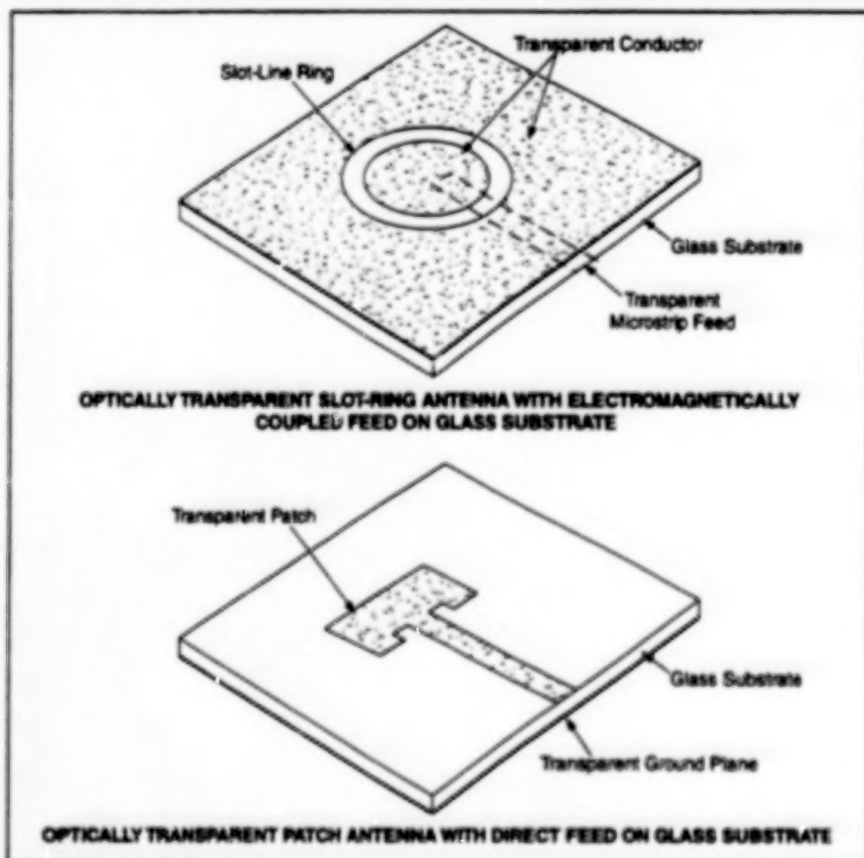
Figure 2. **Conductive Transparent Films on Glass Substrates** can be deposited through photoresist masks in patterns required for antenna patches.

Optically transparent patch antennas have been invented for use in communication systems at frequencies of the order of a few gigahertz. These antennas can be mounted on windows of buildings and vehicles, on computer video monitors, on solar photovoltaic panels, and on other convenient supports; this is an advantage in situations in which the reuse of such supports for radio communication is dictated by a lack of room for adding separate antenna-supporting structures. Another advantage of the optically transparent patch antennas is that they weigh less than conventional antennas do.

An optically transparent patch antenna can be made from an optically transparent, electrically conductive film deposited on one face of a polyester film or a glass substrate; e.g., AgHT, or equivalent. In the case of a polyester film (see Figure 1), the deposited layer has a surface resistance of 6 to 10 ohms per square. The patch and its feed strip can be formed simply by cutting the coated film in the required pattern.

Typically, the polyester film is 0.0075 in. (0.19 mm) thick and is supported over a ground plane by an intervening nonconductive transparent film 0.0035 in. (0.089 mm) thick. Thus, the total thickness of dielectric material supporting the antenna patch is 0.011 in. (0.28 mm). The purpose

of increasing the dielectric thickness by use of the intervening film is to increase the antenna bandwidth. Of course the fabrication of such an antenna on polyester film offers the advantage that the antenna can be bent to conform to a curved support.

Figure 2 presents examples of optically transparent patch antennas on glass substrates. Typically, a glass substrate is about 0.0115 in. (0.292 mm) thick and the deposited conductive film has a surface resistance of about 2.8 ohms per square. Whereas a polyester film must be cut to the required pattern, the conductive film on a glass substrate is patterned by depositing the conductive material through the open areas of a photoresist mask.

In tests, prototype optically transparent patch antennas like those shown in Figures 1 and 2 were found to exhibit radiation patterns, return losses, and input impedances similar to those of conventional patch antennas made from copper conductors. The observed radiation patterns are considered to be good for wireless communications, and the input impedances are well matched to the practical and commonly sought value of 50 ohms.

Array Detector for Charge-Detection Mass Spectrometer

Multiple smaller electrodes perform better than does a single larger electrode.

NASA's Jet Propulsion Laboratory, Pasadena, California

The pixelated array detector (PAD) is a planar array of complementary metal oxide/semiconductor (CMOS) charge-collecting electrodes and readout circuitry for measuring the electric charges on particles in a charge-detection mass spectrometer (CDMS). In comparison with a single-Faraday-cup detector occupying the same total area, the PAD offers advantages, as explained below.

The CDMS approach offers a faster, cheaper alternative to pulsed gel electrophoresis and other techniques for measuring the masses of a variety of large molecules (masses > 10^6 daltons) and similarly sized particles. Examples of particles amenable to CDMS analysis include polymer molecules, bacteria, viruses, and airborne contaminant particles. Whereas a typical analysis by pulsed gel electrophoresis takes days, a typical analysis by CDMS takes minutes.

In a CDMS, a particle to be analyzed is first subjected to electrospray ionization, causing it to bear an electric charge as high as hundreds of thousands of fundamental (electron) units. The particle is then accelerated electrostatically into a Faraday tube connected to circuitry for measuring the time of flight of the particle along the tube. Upon leaving the Faraday tube, the particle impinges on a charge-collecting electrode or else enters a Faraday cup, the electrode or cup being connected to a charge-sensitive amplifier. The time of flight through the Faraday tube is related in a known way to the charge-to-mass ratio of the particle. Thus, the mass of the particle can be calculated from the Faraday-tube time-of-flight measurement and the measurement of collected charge.

The collection area and thus the fraction of ions collected increases with the size of
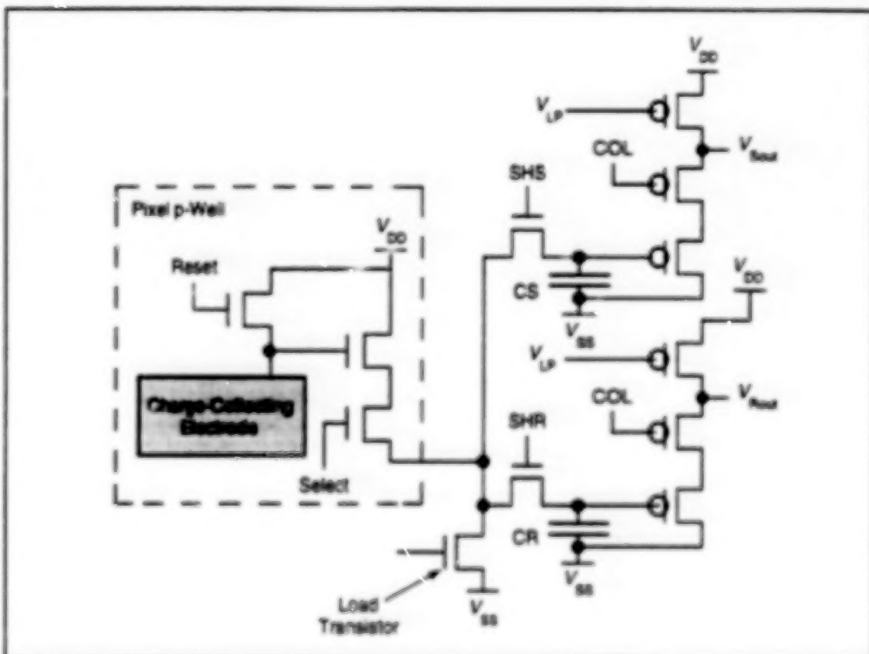
One Pixel Circuit and part of the circuit common to all pixels in a column is depicted in this abbreviated schematic diagram.

the charge-collecting electrode, but the capacitance and associated electronic noise also increase with size. This leads to the basic idea of the PAD, which is to use a sufficiently large total charge-collection area to obtain the desired charge-collection efficiency while apportioning the area among multiple small electrodes or Faraday cups for measurement of the charge deposited into them. Because each electrode occupies a small fraction of the total charge-collection area, the capacitance and electronic noise are reduced accordingly.

A proposed CDMS containing a PAD would include an optional electrostatic deflector, which, when triggered by the passage of an ion through the tubes, would prevent additional ions from reaching the PAD until the PAD had been read out and reset. The ion-passage-induced trigger signal would also be used to gate the readout of the pad to reduce the noise associated with collection of dark current. The time needed to clock the flight of a single ion and measure its charge should be no longer than a few milliseconds; thus, it should be possible to measure a hundred or more ion masses per second and to accumulate a complete mass spectrum with data on thousands of ions in less than 30 seconds.

A prototype PAD contains a 28-by-28 array of pixels with a 40-by-40-μm pitch. The charge-collection electrode of each pixel is a 36-by-36-μm metal patch on its

surface. Each pixel (see figure) contains a source-follower input transistor, a row-selection transistor, and a row-reset transistor. At the bottom of each column of pixels there is (a) a load transistor, (b) an output branch containing a sampling switch (SHS) and sample-and-hold capacitor (CS) for storing signal levels, and (c) a similar output branch with a switch (SHR) and sample-and-hold capacitor (CR) for storing reset signals. There are also source followers with a column-selection switches (COL) at both ends of each column. The reset and signal levels are read out differentially, suppressing fixed pattern noise. If signal levels are read out twice — once before and once after integrating charge — then kTC noise (where k is Boltzmann's constant, T is absolute temperature, and C is capacitance) is also suppressed. In tests, the prototype PAD exhibited a noise floor of 90 electrons root mean square at room temperature.

*This work was done by Stephen D. Fuerstenau and George A. Soli of Caltech for **NASA's Jet Propulsion Laboratory**. Further information is contained in a TSP [see page 1].*
NPO-20128

Alternative One-Time-Opening Miniature Isolation Valve

Valves like this one could be used in microspacecraft propulsion and chemical analysis.

*NASA's Jet Propulsion Laboratory,
Pasadena, California*

The figure depicts a proposed miniature, electrically actuated, one-time-opening isolation valve that would be made mostly of silicon, by use of micromachining techniques. Isolation valves are needed in systems in which fluids must be stored for long times until use, with no leakage or contamination prior to release. Miniature isolation valves like this one could serve to control the release of propellant liquids or gases in microspacecraft, or of stored chemical reagents in portable *in situ* chemical-analysis apparatuses. Eventually, such apparatuses may include one-time-use biochemical-analysis chips.

The proposed valve would function similarly to the one described in "One-Time-Opening Miniature Isolation Valves" (NPO-19927), *NASA Tech Briefs*, Vol. 21, No. 2 (February 1997), page 4b. However the design and thus the details of the micromachining process would differ. Like the previously reported valve, the proposed valve would contain a flow channel blocked by an electrically conductive barrier made of doped silicon. Metal electrical leads would connect the barrier with a valve-opening electrical circuit. To open the valve, the circuit would supply enough electrical current to melt the barrier. The pressurized upstream fluid released by melting of the barrier would carry the barrier debris downstream. A filter downstream of the barrier site but upstream of the outlet would capture the debris.

The overall dimensions of the valve would be about 10 by 10 by 2 mm. The valve would comprise three layers that would be micromachined individually, then assembled and bonded. The middle layer would be a silicon-on-insulator (SOI) wafer that would comprise three sublayers: an upper bulk silicon sublayer several hundred microns thick, a middle oxide insulating sublayer a few microns thick, and a lower doped silicon epilayer some tens of microns thick. The SOI wafer would be microma-

EXPLODED VIEW

CROSS SECTION (not to scale)
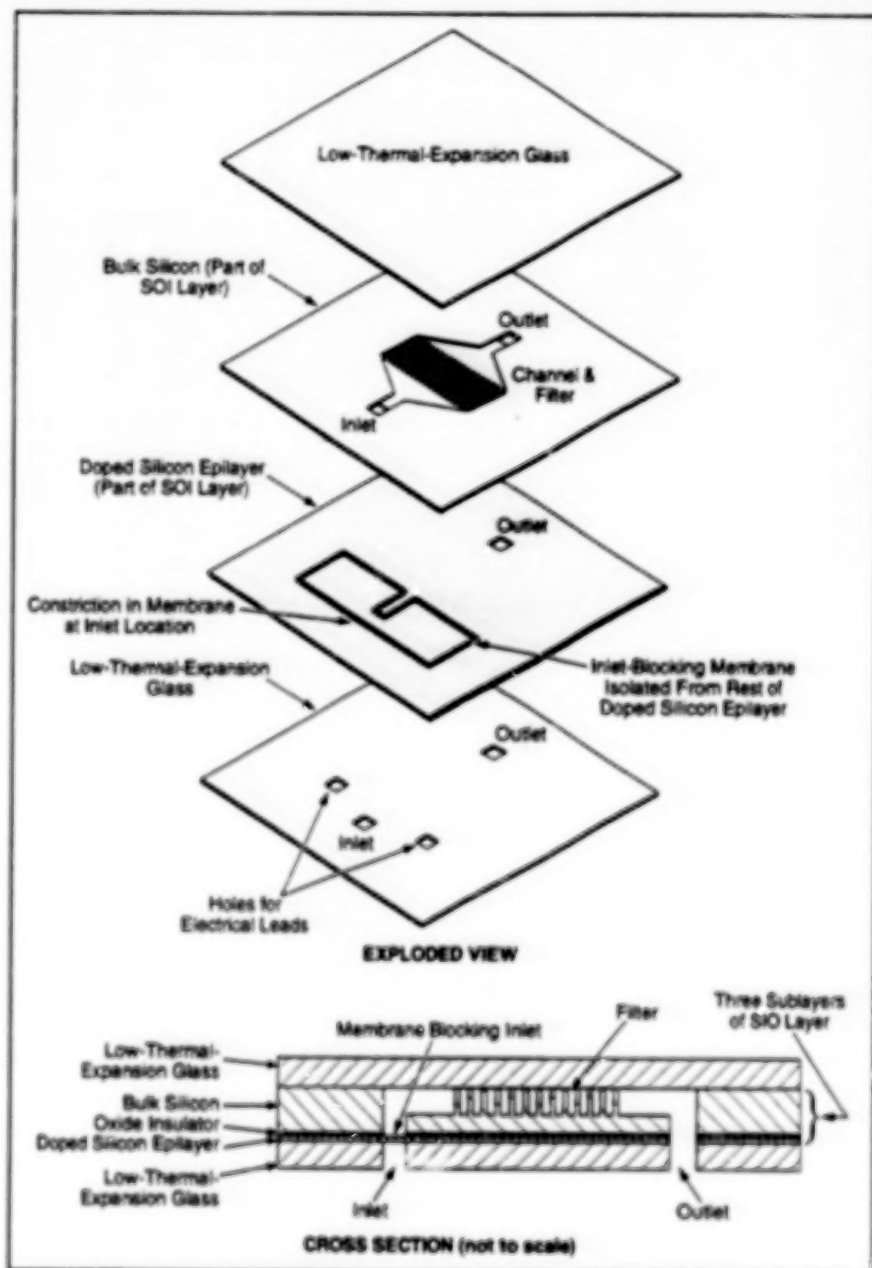
The **Doped Silicon Membrane Blocking the Channel** would be melted electrically to open the channel. According to the concept reported in the noted prior article, a channel would be blocked by a silicon plug doped through part of its thickness. Unlike the plug, the membrane in this design would be likely to melt completely.

chined from both sides to create an inlet sealed by an epilayer membrane, an outlet, a channel between the inlet and the outlet, and a filter in the channel. The top layer — a wafer of low-thermal-expansion glass — would be anodically bonded to the top surface of the SOI wafer to seal the channel. The bottom layer would be another low-thermal-expansion glass layer containing micromachined openings for the inlet, outlet, and two electrical leads. The bottom glass layer would be anodically bonded to the bottom surface of the SOI layer.

The SOI layer would be the most complicated part of the valve; micromachining

of the SOI layer would involve several steps. By means of a patterned etch of the bottom surface of the SOI layer, the portion of the doped silicon epilayer in the outlet region would be removed, while a strip of the doped silicon epilayer in the inlet region would be isolated to form the membrane covering the inlet and extending between electrical contacts. (This membrane would constitute the barrier to be melted by electrical heating. A constriction in the membrane at the inlet location would ensure concentration of electrical heating in the portion of the membrane blocking the flow channel.) Then by means of a patterned

etch from the top surface of the SOI layer, holes for the inlet, outlet, and electrical leads would be formed through the thickness of the thick silicon sublayer. The channel between the inlet and outlet, containing an integral filter, would be formed in still another patterned etch.

This work was done by Indrani Chakraborty, Juergen Mueller, Andrew Wallace, and Wen Li of Caltech for **NASA's Jet Propulsion Laboratory**. *Further information is contained in a TSP [see page 1].*
NPO-20473

Circuit Detects Pyrolysis of Polyimide Insulation on Wires

This circuit can also be modified to prevent further pyrolysis.

Lyndon B. Johnson Space Center, Houston, Texas

An electronic circuit has been designed as a prototype of a device that determines whether critical electrical systems have been compromised because of pyrolysis of polyimide-insulated wires. This circuit can be modified to prevent further pyrolysis and to check for indications of pyrolysis for a wide variety of load resistances and power supplies. Circuits like this one could be beneficial in spacecraft, in military and commercial aircraft, and in the nuclear power industry where polyimide-insulated wires are used.

The device is divided into two main sections: a pyrolysis-detection circuit and a potential-pyrolysis-indication circuit. The heart of the pyrolysis-detection circuit is an instrumentation amplifier that monitors the voltage drop across a shunt resistor as current flows through the resistor to a load resistance. If polyimide-insulated wire in

series with the load resistance begins to pyrolyze, the current through the shunt resistor begins to increase. If the current exceeds a preset value (in the present design, 1.50 A, corresponding to a pyrolyzed-polyimide resistance value of approximately 35 Ω), then the instrumentation amplifier puts out a signal with a potential of approximately 1.10 V to the inverting input pin of a comparator. The output potential is set to this level by adjusting a gain resistor while 1.50 A of current is flowing through the shunt resistor. When the comparator (which is configured with a threshold voltage of approximately 850 mV) is triggered, a transistor is turned off, thereby disabling a solid-state relay and interrupting the flow of electrical current to the load and the pyrolyzing wire.

After the pyrolysis event has passed, the circuit then tests the pyrolyzed wires and

adjacent wiring to determine whether any wires are hazardous. This involves routing the output from a precise 5-mA current source through the load and the low resistance of the pyrolyzed wire. A potential unsafe pyrolysis condition is detected by use of an operational amplifier configured as a comparator with a trigger threshold voltage that corresponds to a critical pyrolysis resistance of approximately 35 Ω. After the threshold voltage has been reached, a transistor becomes turned on, causing illumination of a light-emitting-diode display to indicate the potential unsafe pyrolysis condition in the wiring under scrutiny.

This work was done by Timothy E. Roth of Allied Signal Technical Service Corp. for **Johnson Space Center**. *Further information is contained in a TSP [see page 1].*
MSC-22717

12

Electronic Systems

Hardware, Techniques, and Processes

14

# M-JPEG Video Compression System for Space-Based Applications

This video-compression/decompression system meets the unique demands of space-based applications.

Lyndon B. Johnson Space Center,
Houston, Texas

An M-JPEG video compression system has been modified to satisfy the unique requirements of space-based applications. ["M-JPEG" signifies the still-image-data-compression method of the Joint Photographic Experts Group (JPEG) as applied to moving (e.g., video) images.] This ruggedly constructed, modular system is compatible with NASA interfaces and meets Agency requirements for reduced size, weight, and power. The M-JPEG system generates test patterns, enables users to select compression characteristics and desired output rate, is inexpensive to modify and upgrade, and has features that are adaptable to mission-specific requirements.

Two categories of video compression/decompression systems are commercially available: (1) computer-based video compression/decompression systems for multimedia applications and (2) stand-alone box compression/decompression systems for broadcast applications. None of these systems satisfies the requirements for all of NASA's unique applications. The sizes, weights, and power demands of commercial video systems are too high. Commercially available systems also do not provide compatible interfaces or compression options that users can select and control from front panels, and they do not generate test patterns. Moreover, most commercial compression/decompression systems are not ruggedly constructed or modular in design, many do not provide adequate video quality, and none is capable of adjustment to any desired output rate. Finally, the cost of retrofitting any of these systems to satisfy NASA requirements is prohibitive. To summarize: While the video compression/decompression systems currently in use satisfy the commercial industry requirements for which they were designed, they fail to meet NASA's unique requirements for space-based applications.

The M-JPEG system has been designed to perform functions specific to space flight. It was modified to enable it to perform the following functions: digitize a standard SMPTE-170M National Television Systems Committee (NTSC) signal using a variety of programmable color spaces; compress a digital video signal using an adaptive M-JPEG compression algorithm; enable the user to select compression modes and thereby modify compression parameters; packetize the compressed digital video signal for transport; provide both a fiber-optic
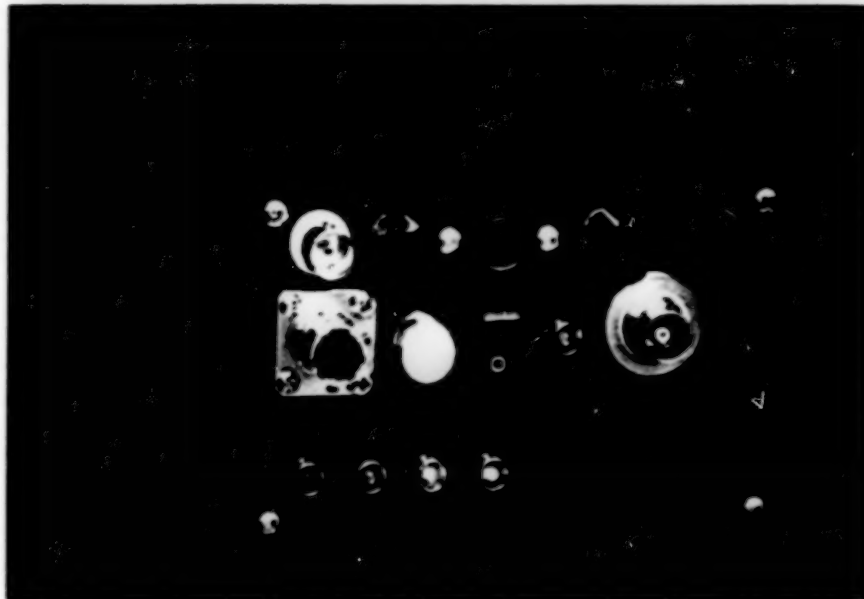
The **Compression Subsystem of the NASA M-JPEG Video System** contains the M-JPEG video encoder plus a video digitizer, a packetizer, and a power supply.

and an electrical [emitter-coupled logic (ECL)] output interface; receive the compressed digital video signal, decompress the data, and produce an acceptable version of the original noncompressed digital video signal; and convert the decompressed digital video to a variety of formats for display [e.g., red, green, blue (RGB), composite NTSC, or component NTSC (Y/C)]. This range of capabilities enables NASA to: (1) improve the quality of video transmissions over that of standard analog video transmissions, (2) transmit multiple video channels within bandwidths previously needed for one channel, and (3) make efficient digital recordings of compressed digital video signals and multiple-generation recordings without degradation.

The M-JPEG video system consists of two primary subsystems: the onboard compression system and the ground-based decompression system. The figure shows the onboard compression system, which contains the M-JPEG video encoder. This encoder is housed in an anodized aluminum case that contains the printed-circuit boards (PCBs). There are four such PCBs: (1) a video digitizer, (2) the M-JPEG encoder, (3) a packetizer, and (4) the power supply. Many components of this subsystem are programmable logic devices; these include an erasable programmable read-only memory (EPROM), erasable programmable logic devices (EPLDs), and a stand-alone microsequencer (SAM).

The M-JPEG video system is designed to interact with either the high-frame-rate multiplexer (HRFM) of the International Space Station or with a space shuttle multiplexer. Because of the modular design of the onboard compression system, three of the PCBs — the video digitizer, the M-JPEG encoder, and the power supply — can be retained in their original state, while an alternate communication circuit can then be employed instead of the packetizer to serve as an interface with another system.

The ground subsystem consists mainly of three personal computer (PC) advanced technology (AT) Industry Standard Architecture (ISA) boards. The user connects the display circuit to either a red/green/blue (RGB) NTSC monitor or to a composite NTSC or component Y/C monitor, depending on which of the two display circuits is being used. Several programs are utilized to initialize the PC AT boards and run the ground system. Programs have been written to read the telemetry data to determine the configuration of the onboard system. The settings of the ground-system boards can be read to ensure that the proper configurations and frames can be captured whenever the user wants to import an image into the ground computer. (The current file format for imported images is the Targa 24 image file format.) Because of the limitations of the PC AT ISA bus and the enormous amount of storage capacity

needed to store even a short video sequence of the required quality, the system does not allow storage of compressed motion video data in the ground computer. The M-JPEG video system can be used to provide broadcast-quality video to an existing analog video ground distribution system or, preferably, to a digital video ground distribution system. Decoding is done at the end viewing location.

The M-JPEG video is flexible enough to be amenable to modification, to satisfy a variety of requirements and to suit various applications. For example, computer interfaces could be changed to enable the use of the ground-based components of the system with alternate computers. Inasmuch as the onboard system is modular, it can be modified for different interfaces, as for different communication protocols. A system currently under development — the Moving Pictures Expert Group (MPEG) 2 codec — will incorporate the video digitizer and packetizer from the M-JPEG system, but the encoder board will be replaced with circuitry that implements an alternate compression algorithm.

While the concepts included in the design of the M-JPEG video system are not new, specific implementations of the design are new. The combination of existing techniques and equipment is unique and satisfies the similarly unique requirements of NASA's space-based applications.

This work was done by S. Douglas Holland of **Johnson Space Center**. *Further information is contained in a TSP [see page 1].*
MSC-22744

Wireless Information Network

A wireless information network (WIN) is undergoing development for use by workers at locations scattered across Kennedy Space Center (KSC). This WIN could be a prototype of a larger network that would serve all of NASA; by logical extension, it could also be a prototype of commercial WINs. By use of a combination of commercial hardware and custom software, this WIN would give KSC personnel access to the main KSC information systems, electronic mail, and other productivity-enhancing computational capabilities. The software includes the IPSWITCH application program, which is compatible with the Windows 3.1, 95, and NT operating systems. IPSWITCH enables the user to store several network-configuration profiles for a computer work station, making it possible to reconfigure the computer rapidly to operate on different subnetworks. When the user starts the execution of IPSWITCH under Windows, the program generates an interactive display, through which the user can create, edit, and save five different Internet Protocol (IP) configurations for each subnetwork interface.

This work was done by Mark Sullivan for **Kennedy Space Center**. *For more information please contact Kevin Jackson at Sentel Corporation, 225 Reinekers Lane, Suite 500, Alexandria, VA 22314, Tel No. (703)739-0084 or e-mail kjackson@sentel.com*
KSC-11964
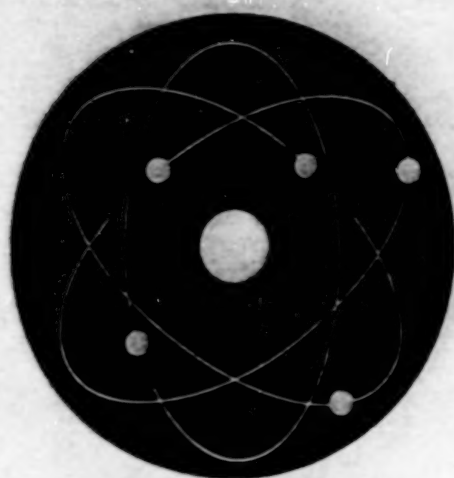
Physical Sciences

Hardware, Techniques, and Processes

Books and Reports

18

Forward-Scattering Particle-Image Velocimetry

Using only one line of sight, one can measure three-dimensional velocity.
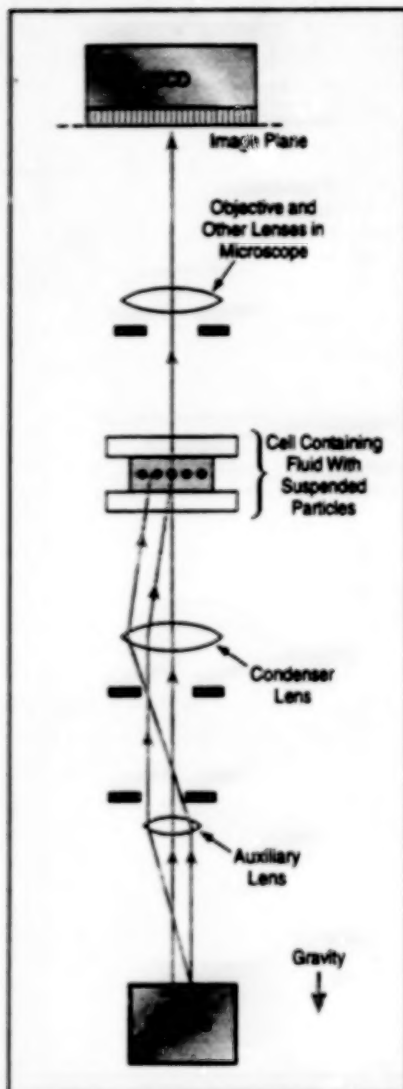
John H. Glenn Research Center,
Cleveland, Ohio

Figure 1. **A Microscope Resolves Forward Scattering** of partially coherent light from particles suspended in a fluid. The magnified image is captured by a CCD.

Forward-scattering particle-image velocimetry (FSPIV) is a technique for measuring velocities in microscopic flow fields as thin liquid films. As in other particle-image-velocimetry (PIV) techniques, the velocity of a flow is computed from temporaly changing images of suitably illuminated, neutrally buoyant particles entrained in the flow. Unlike other PIV techniques, (1) particles are back-illuminated with coherent or partially coherent light, (2) a microscope is used to resolve forward scattering of light from the particles, and (3) all three components of velocity can be measured from only one line of sight, without readjustment of optics.

Figure 1 illustrates a laboratory setup for FSPIV. Illumination is provided by a microscope-illumination source equipped with a wavelength-selective filter. Partial coherence is obtained by closing the aperture on the illumination source. Microscopic spherical seed particles of known diameter are suspended in the liq-
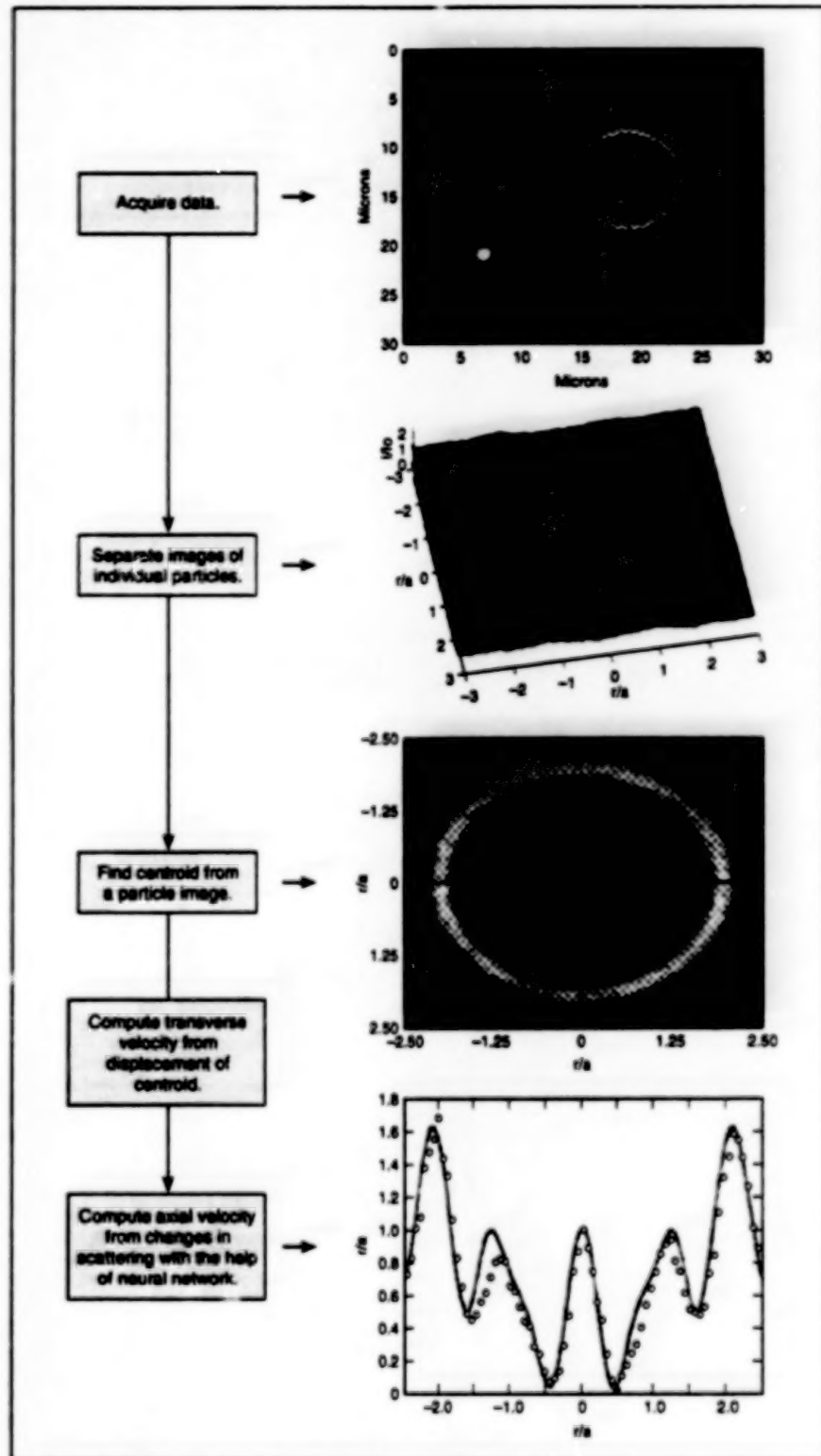

Figure 2. **Magnified Images of Particles** in forward-scattered light are processed to extract data on three-dimensional velocity.

uid. A transmitted-light microscope is aimed through the cell back toward the source and is focused to a suitable depth within the cell. Forward-scattered light from a particle in the field of view of the microscope is brought to focus on the microscope image plane to obtain a magnified image of the particle. A charge-coupled device (CCD) is mounted at the image plane to acquire the image. The CCD output is digitized, then processed as described below to extract information about the three-dimensional velocity of the particle.

Coherent illumination is needed because it makes the forward scattering of light (including such effects as diffraction from particles and phase changes in microscope lenses) amenable to analysis. Highly coherent illumination like that provided by a laser results in speckle noise; partially coherent illumination is preferred in this application because it can yield diffraction patterns adequate for analysis while generating much less speckle noise.

Figure 2 schematically illustrates how images are processed to extract velocities. First, a frame of image data is acquired at a known sampling time. Next, the image of each particle is separated from other particles. The scattering pattern for each particle is analyzed to determine the distance of the particle, relative to the focal plane, along the line of sight. This aspect of the analysis involves comparisons of the observed scattering pattern with scattering patterns that have been computed theoretically and/or recorded experimentally for known positions relative to the focal plane. The comparisons and the interpolations between known positions can be performed by neural-network software that has been trained on the known scattering patterns. Then the component of velocity of each particle along the line of sight is calculated as the distance between two positions determined in this way for two sampling instants, divided by the time between the instants.

The components of velocity in the plane perpendicular to the line of sight are determined by tracking particle-image centroids as they move across the field of view between successive frames. The tracking of particle-image centroids as a function of time is an established PIV practice; techniques for tracking particle-image centroids as functions of time have been reported in a number of previous articles in *NASA Tech Briefs*. An added benefit of FSPIV is that the scattering is centro-symmetric so that the centroid is found with high accuracy.

This work was done by Ben Ovryn of NYMA, Inc., and John D. Khaydarov of Ohio Aerospace Institute for Glenn Research Center. Further information is contained in a TSP [see page 1].

Inquiries concerning rights for the commercial use of this invention should be addressed to NASA Glenn Research Center, Commercial Technology Office, Attn: Tech Brief Patent Status, Mail Stop 7–3, 21000 Brookpark Road, Cleveland, Ohio 44135. Refer to LEW-16403.

Imaging System With TDI and a Two-Axis-Scanning Mirror

A unique optomechanical scanning subsystem offers several advantages.
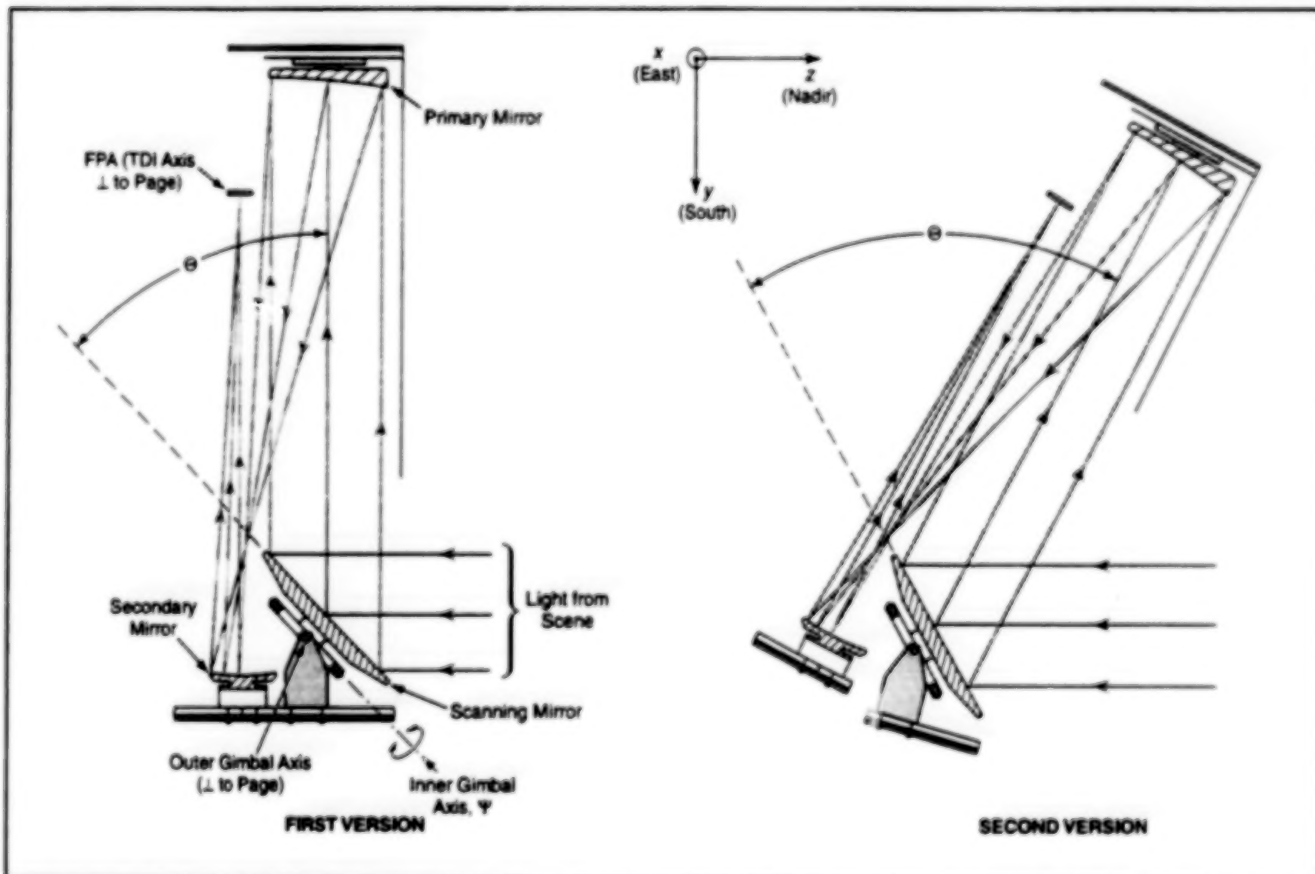
Goddard Space Flight Center, Greenbelt, Maryland

Figure 1. **Both Versions of the System** are based on the same optomechanical design principles. The second version offers some advantages over the first version.

A telescopic imaging system that includes an optomechanical scanning subsystem is undergoing development. The system is designed for use in scientific observation of the Earth from aboard a satellite in geostationary orbit. The basic principles of the optomechanical scanning subsystem may also be applicable to special-purpose terrestrial optical instruments.

The principal optical component of the optomechanical subsystem is the scanning mirror — a flat mirror with an elliptical cross section. The mirror is rotated about two mutually perpendicular axes to scan the focal plane of the telescope in a raster pattern that defines a field of regard that extends across the surface of the Earth and into adjacent areas of dark space (observations of adjacent dark space provide instrument background readings that can be subtracted from Earth-surface readings). The use of the scanning mirror makes it unnecessary to rotate the relatively massive telescope to scan this field of regard, which is wider than the field of view of the telescope. The use of a scanning mirror for such a purpose is not new or unique; instead, the unique aspect of the optomechanical subsystem lies in some of the particulars of its design.

The system (see Figure 1) is most readily characterized by reference to a Cartesian coordinate system. The central line of sight of the field of regard is along the nadir (the z axis). In the first version of the system, the optical axis of the telescope is parallel to the south (y) axis; in the second version, the optical axis of the telescope is tilted 30° from the y axis in the y,z plane. The image is detected on a focal-plane array (FPA) of photodetectors arranged in rows of pixels along the x axis. The along-scan (east–west rapid-scan) component of the raster pattern corresponds to motion of the focal spot along a row of pixels in the x direction. The FPA-readout scheme is based partly on time delay and integration (TDI); this produces a requirement that the optomechanical-scanning velocity be constant and equal to the electronic-scanning velocity so that the packet of charge from each pixel on the FPA will correspond to a line of sight to a single spot in the scene.

The scanning mirror is mounted on a gimbal with two perpendicular axes. The outer axis is attached to the telescope body and is parallel to the x axis; this axis is used to generate the cross-scan component of the raster pattern (north-to-south steps between scanning arcs). The mirror is mounted on the inner axis, which is perpendicular to the outer axis
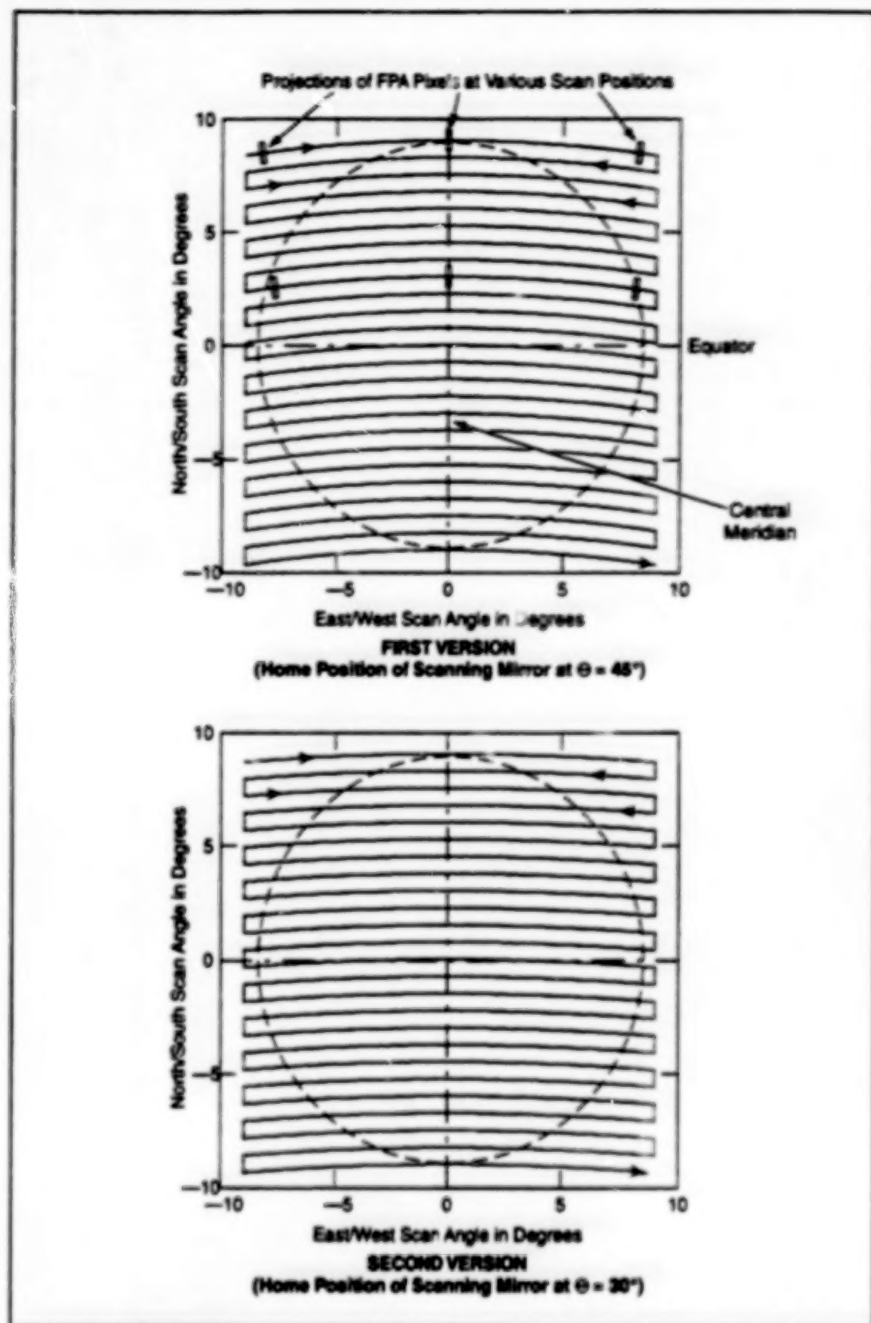

Figure 2. The Earth and Nearby Space Are Scanned in a series of predominantly east–west arcs separated by small north–south intervals. By virtue of the different instrument geometry, the arcs in the second version are more nearly straight lines.

and is used to generate the rapid east–west scan component. In the first version of the system, the angle, θ, between the telescope's optical axis and the inner axis of the scan mirror is 45° at the center of the raster pattern, and decreases from 49.35 to 40.65° as the line of sight (LOS) is scanned from the North Pole to the South Pole (from +8.7 to –8.7° elevation at geosynchronous altitude). In the second version of the system, the angle θ is 60° at the center of the raster pattern and decreases from 64.35 to 55.65°.

The along-scan components of the raster pattern can be described as a series of predominantly east–west arcs separated by small cross-scan north–south intervals (see Figure 2). Each arc is scanned by rotation of the inner axis at constant angular speed to obtain the required constant speed of scanning of the focal spot along a row of pixels. The outer axis is held stationary during the motion along each arc. At the end of each arc, the outer axis is actuated to index to the next north–south position and the arc at that position is scanned along a reverse path by rotating

the inner axle in the opposite direction.

The angular velocity of the LOS equals the rotational velocity of the inner gimbal axis, $d\Psi/dt$ multiplied by $2\sin(\theta)$. The value of $2\sin(\theta)$ decreases on each consecutive arc from north to south, so $d\Psi/dt$ must be increased from arc to arc. The image of the FPA rotates so that its TDI axis always coincides with the scan velocity, and its cross-scan

axis (the long axis) is always perpendicular. (Refer to the top arc in Figure 2.)

The second (30°) version offers several advantages over the first (45°) version:
- The angle of reflection is smaller; consequently, the reflection introduces less spurious polarization.
- The major axis of the mirror ellipse can be made shorter, thereby reducing the mass and angular momentum

of the mirror.
- Rotation of the image (equivalently, rotation of the projection of the FPA pixels onto the scene) is less.

Improved Thermoelectric Converter Units and Power Generators

Rugged, compact TCUs could be used to provide power or cooling in numerous applications.
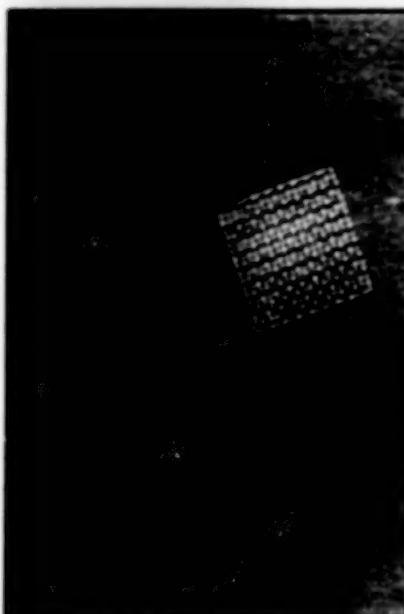
John H. Glenn Research Center, Cleveland, Ohio

Figure 1. A **TCU is a Rectangular Parallelepiped Module** containing p- and n-doped pieces of bismuth telluride in a square array. The cold side is shown here. The overall dimensions of the module are 0.291 by 0.291 by 0.9 in. (7.4 by 7.4 by 22.9 mm).

Figure 2. A **40-mW RTG** would contain a TCU like that shown in Figure 1, plus an RHU of a type that has been used in spacecraft.

Improved thermoelectric converter units (TCUs) and radioisotope thermoelectric generators (RTGs) that contain them have been undergoing development for use as small, lightweight sources of electricity at potentials up to 5 V and power at levels up to 40 mW. These RTGs are intended primarily for supplying power to operate electronic equipment in outer space or at remote or uninhabitable locations on Earth; terrestrial applications could include monitoring of nuclear-waste-storage facilities, meteorological monitoring at polar locations, deep sea exploration, and monitoring of geological activity inside volcanic craters and at underground locations.

In general, a thermoelectric generator includes a TCU plus a source of heat. In the case of an RTG, the source of heat is a
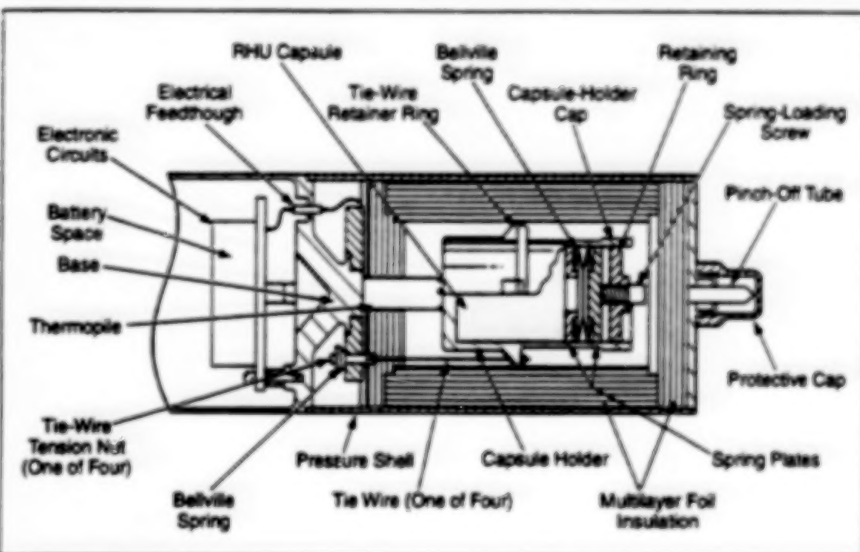
radioisotope heater unit (RHU). The present RTG design is derived partly from the design of 75-mW radioisotope power systems that were built for the United States government in the late 1970s and early 1980s. The present design also incorporates some of the concepts reported in "Miniature Radioisotope Power Source" (NPO-19339) NASA Tech Briefs, Vol. 19, No. 9 (September 1995), page 60. The RHU in the present design generates thermal power of 1 W and is of a type that has been proven in use aboard spacecraft to warm instruments that are sensitive to cold.

Alternatively, the improved TCUs could be energized by nonradioactive heat sources, including sources of waste heat (e.g., household appliances, power tools, camping equipment), small burners (similar to cigarette lighters) that burn hydrocarbon fuels, or any of a variety of other sources that are inexpensive and readily available. Power supplies based on this concept could be used to charge batteries or to

operate low-power electronic equipment under emergency or outdoor conditions, for example. These power supplies offer an important additional advantage in that they could function over wide temperature ranges, including temperatures both above and below the operational temperature ranges of chemical batteries. The improved TCUs could also be used as heat pumps or coolers, especially in electronic equipment; in comparison with conventional thermoelectric coolers, these TCUs would be more durable and could be made smaller.

A TCU is a thermopile made from state-of-the-art thermoelectric materials — in this case, p- and n-doped, vacuum-hot-pressed bismuth telluride. The present developmental TCU is fabricated as a module (see Figure 1) that contains an 18-by-18 square array of alternating p- and n-doped pieces of bismuth telluride separated by pieces of polyimide film. Each element of the array is a square 0.015 in. (0.38 mm) wide. The overall dimensions

of the module are 0.291 by 0.291 by 0.6 in. (7.4 by 7.4 by 22.9 mm). The elements of the array are electrically connected in series by gold contact strips on the hot and cold sides. The design hot and cold junction temperatures are 250 and 25 °C, respectively.

Fabrication of the module involves a process of stacking, cutting, and restacking pieces of the p- and n-doped thermoelectric material and polyimide films, followed by placing the final stack in alignment tooling and vacuum hot pressing the final stack to bond the pieces together. Accurate alignment and proper bonding of the array elements in the stack are prerequisite for the next step, in which the gold contact strips are applied by a

...king/deposition process used customarily in the electronics industry.

Figure 2 is a simplified cross section of a proposed RTG that would incorporate the developmental TCU. The RHU capsule would be contained in aluminum capsule holder, which would be mounted in contact with the TCU and pressed against the TCU by tension in four spring-loaded titanium tie wires. The RHU capsule would be spring-loaded to keep it stationary within the holder in the presence of shock and vibration and to minimize thermal resistance between the RHU and the TCU. A thermally conductive electric insulator (made of boron nitride) would be placed between the capsule holder and the hot side of the TCU to prevent electrical short-

circuiting of the TCU. Thermal insulation for the hot parts of the RTG would comprise multiple layers of aluminized polyimide film interspersed with layers of ceramic paper. The interior of the RTG could be either evacuated or else filled with xenon.

This work was done by John C. Bass of Hi-Z Technology, Inc., and Alex Borshchevsky of NASA's Jet Propulsion Laboratory for **Glenn Research Center**.

Inquiries concerning rights for the commercial use of this invention should be addressed to NASA Glenn Research Center, Commercial Technology Office, Attn: Steve Fedor, Mail Stop 4–8, 21000 Brookpark Road, Cleveland, Ohio 44135. Refer to LEW-16556.

Low-Absorption Color Filters for Flat-Panel Display Devices

Reflected light would be reused to obtain brighter displays.

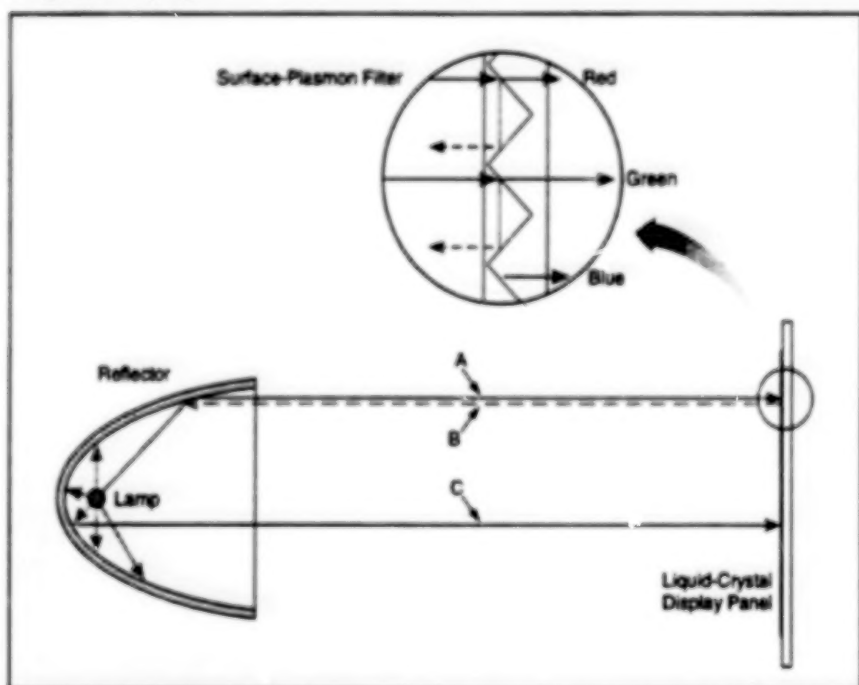NASA's Jet Propulsion Laboratory, Pasadena. California

Figure 1. **Light Not Used in the Display** at a given location would be reflected by a surface-plasmon color filter for use elsewhere. In the example shown here, incident ray A would give rise to reflected ray B, which would be reflected twice by the collimating reflector to become ray C.

Figure 2. Alternating **Rows of Microprisms** in a surface-plasmon color filter in a pixel would transmit and reflect light in mutually orthogonal polarizations. This arrangement would make it possible to utilize both polarization components of unpolarized light, whereas heretofore, only one of them has been utilized.

A proposed technique for color filtering in a liquid-crystal or other flat-panel display device would make it possible to brighten the display without increasing the amount of light supplied from behind the panel. The need for the proposed technique arises as follows: At present, each pixel in a typical color liquid-crystal display device contains three dye filters: red, green, and blue. Each filter transmits its single primary color and absorbs the other colors, so that less than one-third of the available

light is used for viewing. In addition, the liquid-crystal display uses polarized light, so that half of the incident unpolarized illumination is necessarily wasted. The net result is that less than one-sixth of the incident unpolarized light is utilized. One does not have the option of increasing the illumination substantially to brighten the display because the increase in heat generated by absorption of light in the filters could harm the display device.
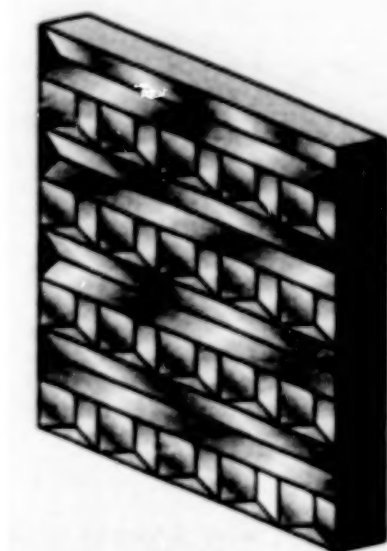
In the proposed technique, one would

replace the dye filters with surface-plasmon or interference filters, which are more reflective than absorptive. In addition, the filter and illumination optics would be arranged so that much of the light reflected from the filters would be reused as illumination. The overall effect should be an increase in brightness and efficiency.

Figure 1 illustrates this concept as applied to a liquid-crystal panel back-lit by a lamp with a collimating reflector. Light

reflected from a color filter on the panel would return to the collimating reflector, where it would be reflected twice and sent to a different location on the panel. Of course, neither the original light from the lamp nor the light reflected from the panel would be collimated perfectly as shown in simplified form in the figure; all incident and reflected beams of light would have some angular spread. This spread would be beneficial in that it would make the illumination

more nearly uniform across the panel.

Figure 2 shows a proposed configuration of an in-pixel surface-plasmon color filter, which would contain long, narrow microprisms in odd-numbered rows and shorter prisms oriented perpendicularly to them in even-numbered rows. Light that was p- or s-polarized to the longer prisms would be s- or p-polarized, respectively, to the shorter prisms. Each prism would pass light of only one polarization and

reflect light of the other polarization. Thus, the polarized light not utilized in each pixel would be sent back to the collimating reflector and redistributed elsewhere on the panel, where some of it would be utilized in other pixels.

*This work was done by Yu Wang of Caltech for **NASA's Jet Propulsion Laboratory**. Further information is contained in a TSP [see page 1].*
NPO-20435

Books and Reports

## Updates on Optical Diagnosis of Fuel Spray Patterns

A collection of three reports presents an expanded discussion of the topic of "Optical Diagnostics of High-Pressure Liquid Fuel Sprays" (LEW-16701), *NASA Tech Briefs*, Vol. 23, No. 3 (March 1999), page 18a. The reports describe experiments in which fuel sprays representative of those in liquid-fueled, high-pressure gas turbine combustors were analyzed by a combination of planar laser-induced fluorescence imaging, planar Mie scattering, and phase Doppler particle analysis. The earliest of the reports ("Fuel Injector Patternation Evalua-

tion in Advanced Liquid-Fueled, High-Pressure, Gas Turbine Combustors, Using Nonintrusive Optical Diagnostic Techniques") was the subject of the noted prior article. The middle report ("Optical Fuel Injector Patternation Measurements in Advanced Liquid-Fueled, High Pressure Gas Turbine Combustors") largely reiterates the information in the earliest one. The most recent report ("Challenges to Laser-Based Imaging Techniques in Gas Turbine Combustor Systems for Aerospace Applications") overlaps somewhat with the other two reports and presents some additional experimental results and interpretation. The three reports are accompanied by a fourth document that summarizes the reports

and emphasizes the importance of using the three mentioned optical diagnostic techniques together to extract maximum information on combustor flow fields.

*This work was done by Yolanda R. Hicks, Robert C. Anderson, and Michelle Zaller of **Glenn Research Center** and Randy J. Locke of Dynacs Engineering Co., Inc. To obtain copies of the reports and the summary document, see TSP's [page 1].*

Inquiries concerning rights for the commercial use of this invention should be addressed to NASA Glenn Research Center, Commercial Technology Office, Attn: Steve Fedor, Mail Stop 4–8, 21000 Brookpark Road, Cleveland, Ohio 44135. Refer to LEW-16882.
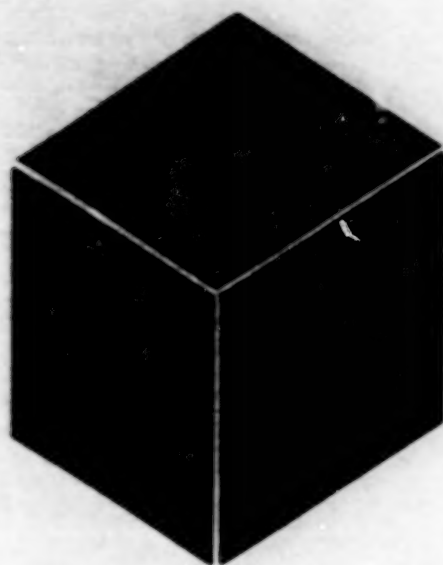
Materials

Hardware, Techniques, and Processes

26

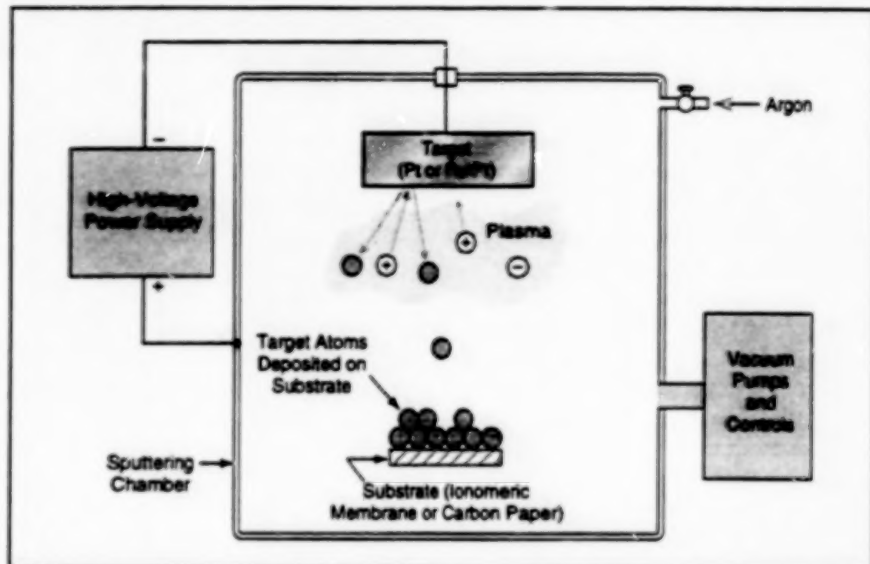# Sputter Deposition of Catalysts for Fuel-Cell Electrodes

Sputtering offers advantages over other deposition techniques.

NASA's Jet Propulsion Laboratory, Pasadena, California

An improved method of fabricating electrodes for fuel cells includes the use of sputtering to deposit thin layers of catalytic electrode metals. Previously, catalytic electrode metals were deposited by means of inks and decals — means that are not amenable to mass production. The sputtering process used in the improved method is better suited to mass production. Sputtering also increases the efficiency of utilization and thereby decreases the needed amounts of the catalytic electrode metals, which are expensive noble metals; whereas the catalyst loadings needed in electrodes made by older methods ranged between 4 and 12 mg/cm^2, the catalyst loadings needed in electrodes made by the improved method range from 0.5 to 1.0 mg/cm^2.

The improved method has been demonstrated in the fabrication of membrane/electrode assemblies for direct methanol fuel cells. Such a membrane/electrode assembly includes a proton-conducting solid-electrolyte membrane sandwiched between two electrode layers. The membrane is made of the ionomer Nafion™ (or equivalent) — a perfluorosulfonic acid-based hydrophilic, proton-conducting polymer. The electrode layers are made of carbon paper coated with catalytic noble metals; Pt for the cathode and an alloy of Ru/Pt for the anode.

Fabrication according to the improved method begins with air drying of the ionomeric membrane for 24 hours, followed by vacuum drying for 30 to 60 minutes. The membrane is mounted in a sputtering chamber, with one side facing up or down toward a target made of one of the noble-metal electrode materials

Sputtering in Argon Plasma is a superior technique for deposition of catalytic electrode metals (Pt and Ru/Pt) on ionomeric and carbon-paper substrates used to make membrane/electrode assemblies for fuel cells.

(see figure). The chamber is evacuated, then backfilled with argon to a pressure between 10 and 50 millitorr (between 1.3 and 6.7 Pa). The sputtering process is initiated by applying a high voltage between the target and the chamber wall. The sputtering process is continued for an amount of time (typically ranging up to a few hours) that depends on the desired catalyst loading. Upon completion of sputtering, air is readmitted to the chamber and the membrane is removed.

The foregoing process is repeated to coat the other side of the membrane with the other noble-metal electrode material. Then using sheets of carbon paper (instead the ionomeric membrane) as the deposition substrate, the process is again

repeated, except that Pt is sputtered into both sides of one sheet of carbon paper, and Pt/Ru is sputtered onto both sides of the other sheet of carbon paper. Both sputter-coated carbon papers are coated with a solution that contains the ionomer in a liquid form. Then the membrane is sandwiched between the coated carbon papers and the sandwich is pressed at a temperature between 140 and 150 °C to obtain a membrane/electrode assembly.

Organic/Inorganic Coats for Packaging of Microelectronics

Thin conformal coats are alternatives to heavier, bulkier conventional hermetic packages.

NASA's Jet Propulsion Laboratory, Pasadena, California

A method for protective packaging of multichip modules and related assemblies of microelectronic circuitry involves coating the assemblies with composite organic/inorganic layers only 1 to 2 mils (0.025 to 0.05 mm) thick. The method is suitable for a variety of advanced packages of microelectronic circuitry, including "chip-on-flex" circuitry, "smart" cards, flip-chips, flip-flips (flip-chips assembled

onto ball grid-array substrates), and such three-dimensional assemblies as stacked memory arrays.

Older methods for protective packaging of electronic circuitry include the following:

• Conventional hermetic sealing in metal or ceramic. This method provides effective protection. However, conventional hermetic enclosures add considerable weight and are relatively bulky [0.15 to

0.25 in. (4 to 6 mm) deep]; thus, conventional hermetic sealing defeats advances in miniaturization.

• Encapsulation in epoxy. Epoxy encapsulants can be applied to depths about one-fourth of those of conventional hermetic packages, but even at these depths, they add unacceptable amounts of weight and bulk. Epoxies are too rigid for use on the new genera-

Inorganic Coating (e.g., Silicon Nitride)

Organic Coating (e.g., Parylene)

Circuit Board

Solder Ball

Coated Flip-Chip Assembly
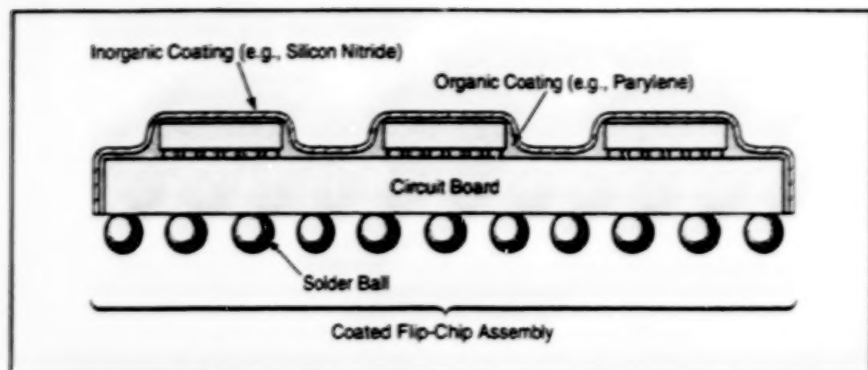
A **Composite Organic/Inorganic Coating** protects the flip-chip assembly at a fraction of the cost of conventional hermetic packaging.

tion of flexible multichip modules. Epoxies are also susceptible to penetration by moisture; in other words, they do not necessarily protect the packaged circuitry against moisture.

• Vapor deposition of a thin film of parylene (a thermoplastic polymer made from para-xylene). Such a film is susceptible to penetration by moisture and to thermal oxidation at temperatures greater than approximately 120 °C.

In the present method, one coats the assembled circuitry with a thin film of parylene, followed by a thin film of silicon oxide or silicon nitride (see figure). Both the organic (parylene) and inorganic (silicon-based) films are deposited at relatively low temperatures (between 25 and 100 °C). The outer inorganic film acts as a barrier to moisture and protects the underlying organic film against oxidation at temperatures up to 200 °C or even somewhat higher. The thin composite organic/inorganic film thus affords almost as much protection as does heavier, bulkier conventional hermetic packaging. The cost of depositing the composite organic/inorganic film is a small fraction of the cost of conventional hermetic packaging.

Although two-layer coats of the type described above are viable, the inorganic outer layers can be broken by mechanical handling. Therefore, it can be desirable to deposit a third (intermediate) layer for protection against mechanical stress (the third layer also provides additional protection against oxidation). For example, one can deposit a base organic layer of Parylene C (a commercial type of parylene), followed by a second organic layer of Cyclotene [or equivalent poly(benzocyclobutene)], followed by an outer inorganic layer.

In the three-layer case described above, one must take special care to cure the second organic layer according to the manufacturer's specifications, to (1) avoid compromising the base organic layer, (2) ensure a full cure to make the second organic layer relatively invulnerable to oxidation, and (3) ensure a smooth, hard second organic layer, over which the final inorganic layer can act as an effective barrier against oxygen. The basic concept can be extended to four or more layers, provided that due consideration is given to adhesion and compatibility between layers. The concept can also be extended to include other materials: For example, other inorganic coating materials that have been considered but not yet evaluated include silicon carbide, silicon oxynitride, and zirconium oxide.

This work was done by Frederick Pool and James Licari of Caltech for **NASA's Jet Propulsion Laboratory**. *Further information is contained in a TSP [see page 1].*
NPO-20304
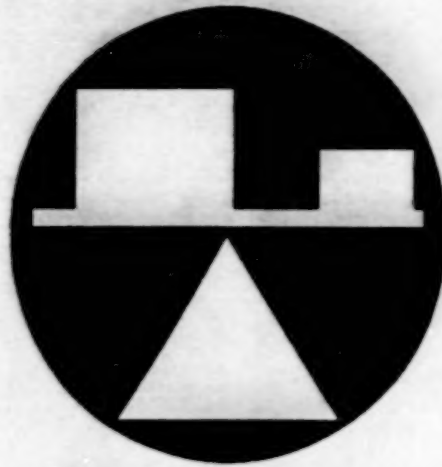
Mechanics

Hardware, Techniques, and Processes

30

Boundary-Layer Rake of Pitot Tubes for Flight Testing

This rake is expected to generate valuable data in forthcoming flight experiments.

Dryden Flight Research Center, Edwards, California

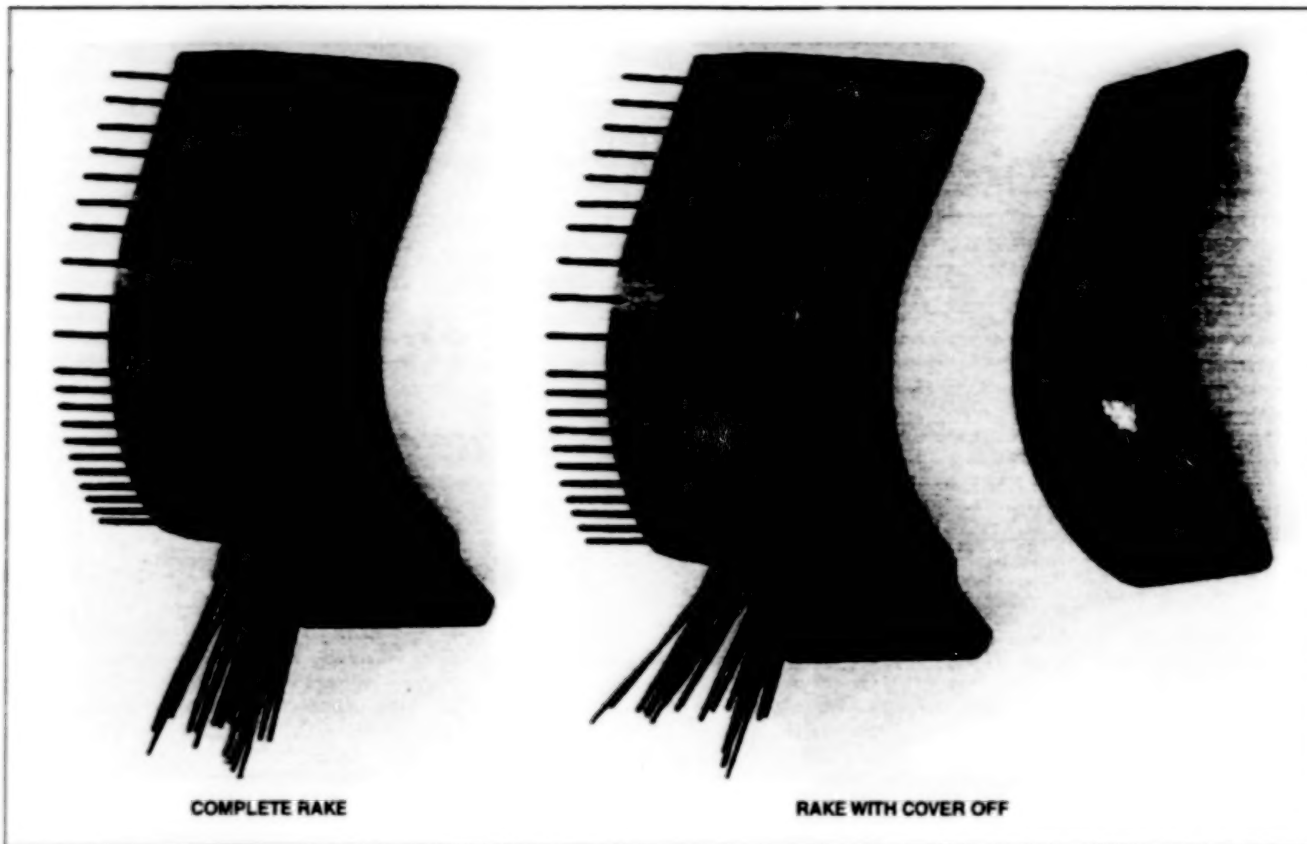**COMPLETE RAKE**   **RAKE WITH COVER OFF**

Figure 1. The **Curved Shape** of the boundary-layer rake makes it possible to cluster the pitot tubes more densely in the near-wall region.

A boundary-layer rake of pitot tubes has been designed and built for installation on a flight-test fixture (FTF) on the NASA Dryden F-15B, which is a two-seat version of the F-15 high-performance, supersonic, all-weather fighter airplane. This boundary-layer rake will be used in flight-research projects in which there are requirements for detailed surveys of the turbulent boundary layer. A design feature unique to this rake is a curved rake body; this feature makes it possible to cluster the pitot tubes in the near-wall region more densely than they can be clustered in conventional rakes. Results of tests have shown that this rake exhibits good aerodynamic performance and that it is operationally rugged.

To give the rake its complex three-dimensional shape (see Figure 1), it was necessary to resort to innovative solid-modeling and machining techniques. Starting from a three-view conceptual sketch, a three-dimensional solid model was constructed by use of the ProEngineer solid-modeling computer-aided design/computer-aided manufacturing (CAD/CAM) software package. This
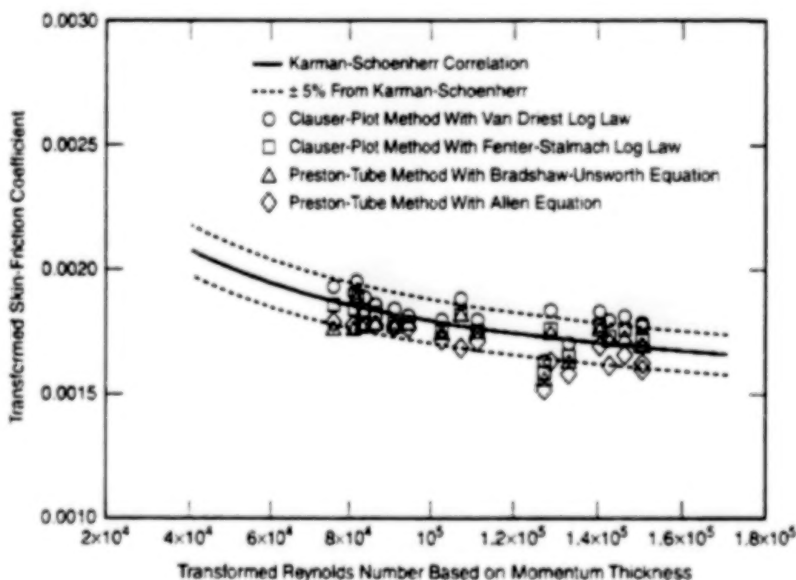

Figure 2. These **Flat-Plate Skin-Friction Data** were calculated from measurements taken by the boundary-layer rake shown in Figure 1.

software package was used throughout the entire design and machining process, ensuring accurate machining of the rake from the three-dimensional solid model. After a solid model was created in ProEngineer, a computer-controlled wire electrical-discharge

machine (EDM) was used to cut the basic shape of the rake out of a solid block of aluminum alloy 2024-T351.

The rake was then machined on a computer numerically controlled (CNC) milling machine. First, the base of the rake was machined for flush mounting on a flat surface. To make room for the installation of the pitot tubes, a cavity was machined inside the rake body. Pitot-tube-mounting holes were drilled on the leading edge of the rake, then the leading edge was tapered to a sharp angle. To close off the cavity in the rake body, an aluminum cover was created on the wire EDM.

After the machining process, all parts were deburred, inspected, and then anodized to provide protection from corrosion and wear. The pitot tubes were machined from 304 stainless steel tubing of 0.04-in. (1.0-mm) outside diameter and 0.0075-in. (0.19-mm) wall thickness that had been annealed to a 1/2-hard condition. The pitot tubes were then inserted in the rake body. The tips of the pitot tubes were chamfered to reduce their sensitivity to local flow angles. A low-viscosity, single-component, anaerobic methacrylate ester adhesive (Loctite 609) was used to hold the pitot tubes in place. To help keep the pitot tubes in place and to protect them from vibrations during flight, room-temperature-vulcanizing (RTV) silicone rubber was used to pot the inside of the rake cavity.

A finite-element stress analysis of the rake design showed very high factors of safety for operation in a supersonic wind tunnel. The rake passed a ground vibration test in which random vibrations of 12 times normal Earth gravitational acceleration were imposed for twenty minutes along each of the three mutually perpendicular directions. A wind-tunnel test of the rake was conducted in the NASA Glenn Research Center 8-by-6-ft (2.4-by-1.8-m) supersonic wind tunnel at mach numbers ranging from 0 to 2. The rake pitot pressures agreed well with data obtained from a conventional rake for the entire range of mach numbers tested. The boundary-layer profiles obtained from the rake data matched the standard log-law profile. As shown in Figure 2, values of skin friction computed from the rake data by use of the Clauser-plot method agreed well with Preston-tube results and with the Van Driest II compressible skin-friction correlation.

The rake will be used in a number of future F-15B/FTF flight experiments. One experiment currently underway is an in-flight evaluation of new skin-friction gauge concepts: the rake data as well as the results from a Preston tube will be used to evaluate the accuracy of new skin-friction gauges. Another experiment is planned to validate the microblowing drag-reduction technique in flight: In this experiment, the net drag reduction caused by blowing an extremely small amount of air through a porous plate will be calculated from the momentum balance of the boundary-layer profiles measured by the rake in the upstream and downstream regions of the porous surface.

This work was done by Trong T. Bui and David L. Oates of **Dryden Flight Research Center**. *Further information is contained in a TSP [see page 1].*

Inquiries concerning rights for the commercial use of this invention should be addressed to the Patent Counsel, Dryden Flight Research Center [see page 1]. Refer to DRC-98-94.
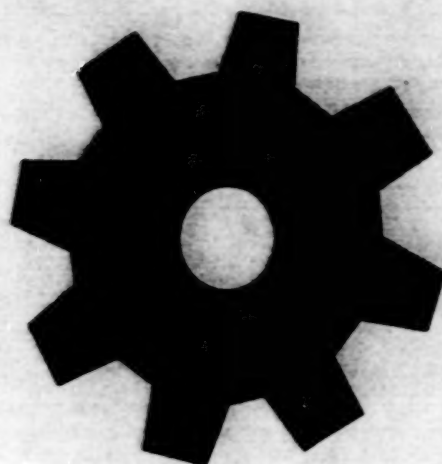
Machinery

Hardware, Techniques, and Processes

34

Improved Magnetostrictive Pump

Features include a two-stage magnetostrictive
actuator and a hydraulic stroke multiplier.

Lyndon B. Johnson Space Center,
Houston, Texas

An improved magnetostrictively actuated
pump has been developed to satisfy a need
for a small, low-pressure, high-flow-rate
fluid pump that contains few moving parts
and can run reliably for long periods without
maintenance. The pump could be used, for
example, to circulate water in the portable life-
support system worn by a firefighter or a
chemical worker or in any setting where relia-
bility is important and maintenance is difficult.
The pump is designed primarily for water
as the pumped fluid, but it could also be used
with other fluids, including cryogenic ones.

The figure shows a meridional cross-
section of the pump. The bottom part con-
tains a magnetostrictive actuator, including
an annular permanent magnet that pro-
vides a constant (bias) magnetic field, and
an electromagnet coil that generates the
variable magnetic field needed for actua-
tion. The magnetostrictive material is the
alloy $Tb_{0.27}Dy_{0.73}Fe_2$ (commercially avail-
able under the trade name "Terfenol-D").

The unusual aspect of the actuator lies in
a two-stage design that approximately
halves the actuator length needed to
obtain a given stroke. There are two pieces
of magnetostrictive material, each 1.5 in.
(3.81 cm) long: a central rod 0.75 in.
(1.9 cm) in diameter, and a surrounding
sleeve of the same volume as that of the
rod. The upper end of the sleeve pushes
against the lower end of the rod via a stain-
less-steel connector, so that the rod tele-
scopes out from the sleeve and the mag-
netostrictive strain of the rod is added to
that of the sleeve to obtain nearly the same
total strain as that of a 3-in. (7.6-cm)-long ,
0.75-in. (1.9-cm)-diameter rod of the mag-
netostrictive material. The connector is
designed to undergo very little strain, rela-
tive to the magnetostrictive strain at the
anticipated actuation loads.

The diameter of the two-stage actua-
tor is greater than it would be with a sin-
gle stage, but this increase in diameter
does not increase the overall diameter of
the pump, because the piston that
effects the pumping action has a greater
diameter. In addition, power consumed
by the two-stage actuator is only slightly
greater than it would be for an equally
capable single-stage actuator.

Above the actuator is a hydraulic stroke
amplifier that includes an outer and an
inner drive bellows. This stroke amplifier
multiplies the actuator stroke by about a
factor of 7.5 [from 2 to 15 mils(0.05 to 0.38
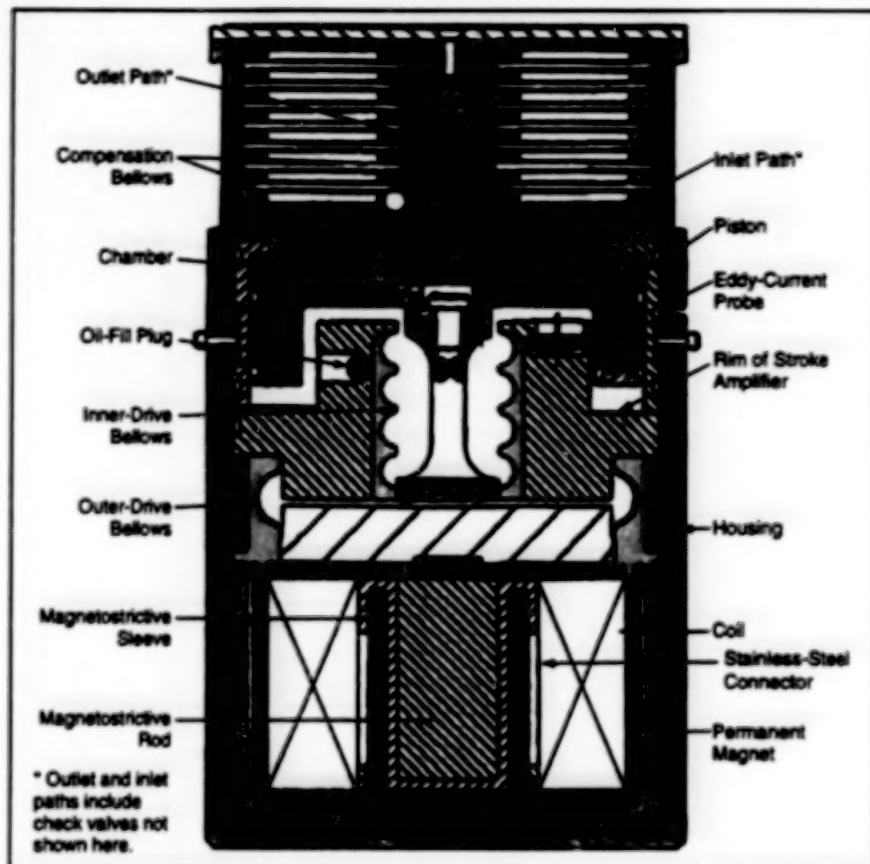
The Improved Magnetostrictive Pump is designed to take maximum advantage of the small
stroke of magnetostrictive actuator. Because this stroke is so small, great care must be exer-
cised in design and assembly to optimize the bias stress on the magnetostrictive components,
and to maximize the rigidity of all components except for the required degrees of compliance
of the bellows and the springs (not shown here) in the check valves.

mm)] while dividing the actuator force by a
factor of 10 in driving the piston. About 75
percent of the work done by the actuator
goes into the output of the stroke amplifier;
the remaining 25 percent is consumed in
compression of the hydraulic fluid and
strain energy of the bellows.

The stroke amplifier drives the piston,
the periodic motion of which draws water
into a chamber through an intake valve
and pushes the water out of the chamber
through an outflow valve. These are light-
weight, fast-response, spring-positioned
check valves. These valves are positioned
to make the water flow circumferentially
around the chamber to obtain a centrifugal
effect that makes trapped air bubbles
accumulate at the center of the chamber,
where they flow out. The accumulated air
must be vented because the pump stroke
is so small that even as little as a few milli-
liters of trapped air greatly impedes perfor-
mance, and more than that amount can

totally block the pumping action.

Above the pump chamber in which the
piston operates there are two compensa-
tion bellows — one on the intake side
and one on the outflow side. These bel-
lows smooth out the flow, reducing the
pulsations that occur at the pump oper-
ating frequency, which is about 24 Hz. If
the pulsations were not smoothed out,
they would give rise to huge forces (water
hammer) that would build up in the water
tubes connected to the pump and there-
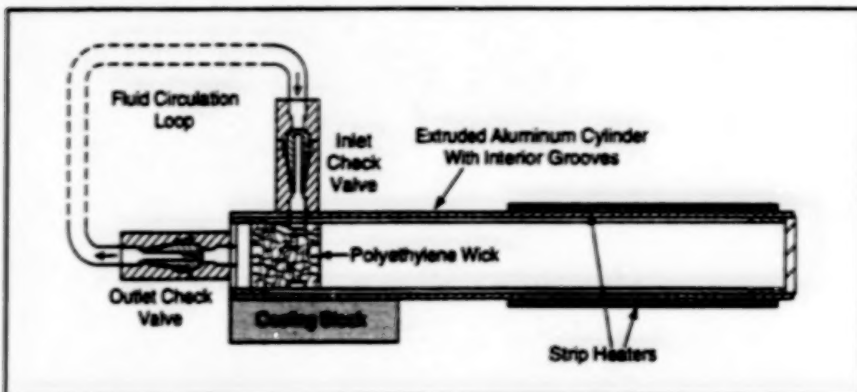by prevent the pump from operating.

The pump is designed to have a flow
rate of 30 milliliters per second and a pres-
sure of 5 psi, and to consume about 25 W
of electric power.

Heat-Driven Pulse Pump

The only moving parts are two check valves.   *Goddard Space Flight Center, Greenbelt, Maryland*

In a **Heat-Driven Pulse Pump**, part of the liquid to be pumped is vaporized, thereby forcing part of the remaining liquid through the outlet check valve. During subsequent condensation of the vapor, liquid enters through the inlet valve. The cycle is then repeated.

The heat-driven pulse pump has been invented in an effort to satisfy a need for pumps that can circulate heat-transfer fluids at low flow rates with high reliability over long operational lifetimes. The heat-driven pulse pump (HDPP) is so named because it generates pumping action by exploiting periodic (pulsed) heating and vaporization alternating with cooling and condensation of the fluid to be pumped. To be amenable to pumping by an HDPP, a fluid must, therefore, be one that can be vaporized and condensed within a convenient range of pressure and temperature. Anhydrous ammonia is one example of such a fluid that could be useful in many applications.

A basic HDPP includes a grooved cylinder, a wick, inlet and outlet check valves, strip heaters, and a cooling block (see figure). The cylinder and other parts are sized to suit the specific application. The two check valves are the only moving parts.

Initially, the cylinder is filled with the liquid phase of the fluid to be pumped. At the beginning of the pumping cycle, power is supplied to the strip heaters for a specified interval of time (pulse). During this interval, some of the liquid in the cylin-der vaporizes. The resulting expansion causes the pressure in the cylinder to rise and the outlet check valve to open. Once the pressure rises to the point where it overcomes the pressure drop in the fluid circuit, the pressure forces some of the liquid through the wick and the outlet check valve; meanwhile, the liquid in the grooves is wicked toward the heater strips and sustains vaporization until the heating power is turned off.

When the heating power is turned off, the vaporization stops. The cooling block is used, if needed, to ensure that during this part of the pumping cycle, the temperature in the cylinder falls to somewhat below the saturation temperature of the fluid-circulation loop. This decrease in temperature causes some or all of the vapor in the cylinder to condense, and the concomitant contraction and decrease in pressure cause the outlet check valve to close and the inlet check valve to open. The vapor is further condensed by the cold liquid that enters through the inlet check valve, so that the wick, grooves, and interior space of the cylinder become refilled with liquid. The system is then ready for the heat pulse that marks the beginning of the next pumping cycle.

A fluid-circulation system can be made to include a pumping subsystem that comprises three HDPPs connected in parallel. To obtain continuous flow in the portion of the fluid-circulation loop external to the pumping subsystem, the three HDPPs are operated in sequence, with two pumps in the recovery (condensation) part of the pumping cycle while the remaining pump is in the pulse (vaporization) part of the cycle.

A prototype system of three HDPPs with anhydrous ammonia as the pumped fluid was tested in experiments. The pressure drop in the fluid-circulation loop was 0.5 psi (3 kPa). A variety of power settings, fluid pressures, timing sequences, and cooling-block temperatures were investigated. The best combination of settings determined in these experiments were a cooling-block temperature of 15 °C, saturation pressure of 28 psia (193 kPa absolute), and heater power of 50 W applied to each pump during 30-second pulses. With these settings, the temperature in each pump varied sinu-soidally between 29 and 35 °C, and the flow rate was 14 grams per minute which would provide 300 W of continuous heat dis-sipation. This combination of settings did not allow any pump to become fully flooded before heating power was resupplied, so that liquid was pushed out quickly when the heat was turned on. This concept would also be applicable to a microgravity environment.

This work was done by Steve Matthew Benner of **Goddard Space Flight Center** *and Mario Santos Martins of Jackson & Tull. Further information is contained in a TSP [see page 1].*

This invention is owned by NASA, and a patent application has been filed. Inquiries concerning nonexclusive or exclusive license for its commercial development should be addressed to the Patent Counsel, Goddard Space Flight Center [see page 1]. Refer to GSC-13739.

Small-Stroke, High-Frequency Reciprocating Pump

Without a sliding piston, the pump could be highly reliable.   *Lyndon B. Johnson Space Center, Houston, Texas*

A proposed reciprocating pump would operate at a small stroke and would contain no sliding parts. The oscillatory motion of a piston in the pump could be provided by a magnetostrictive actuator, for example.

To compensate for its small stroke, the pump would have to operate at a high fre-quency at which most check valves do not work well and at which the pump would be sensitive to trapped air if its piston area were small. Valve efficiency could be increased by use of flapper valves or nozzles. Effective piston area could be increased, without increasing the diameter of the pump, by use of multiple pistons or a helical piston.

This work was done by Arnon Rieger, Michael J. Gerver, Ralph C. Fenn and Dariusz Bushko of Satcon Technology Corp. for **Johnson Space Center**. *No further documentation is available.*
MSC-22462

Axial Force as Indication of Alignment of Threaded Fasteners

A robot would imitate a human technician feeling a thread-engagement click.

<div align="right">Lyndon B. Johnson Space Center,
Houston, Texas</div>
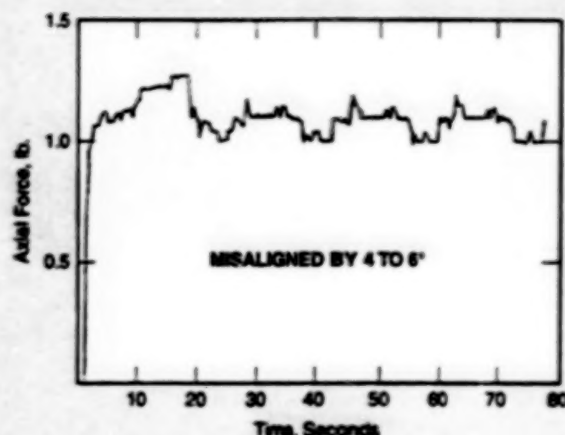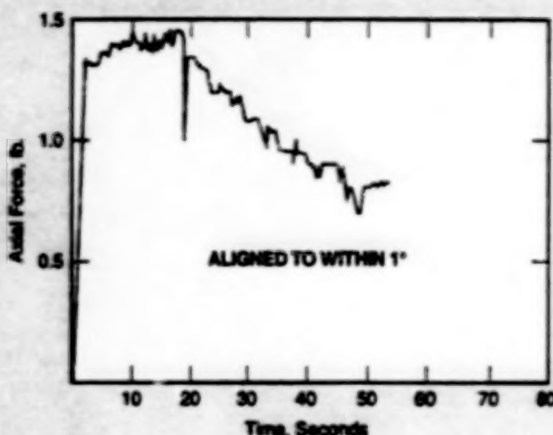
Axial Force between a bolt and a rotating nut was measured by a robot hand that held the bolt.

A developmental technique for automated alignment of threaded fasteners involves the use of the axial force between the fasteners as an indication of alignment. The technique was conceived as a means to guide a robot that is required, for example, to join a bolt with a nut.

The technique is based on the well-known fact that when a bolt and nut are properly aligned, gently pushed together along their common axis, and turned in the loosening direction (counterclockwise for conventional right-handed threads), there is a click — that is, a brief relaxation and recovery of axial force — once per rotation, each time the ends of the threads slip past each other. The technique is also based on the conjecture that the magnitude of the click decreases as the angle of misalignment between the bolt and nut increases.

In a typical application, the robot hand would hold the bolt or nut and would bring it into contact and approximate alignment with its mating nut or bolt, respectively. The robot hand would apply a small preload contact force. Then by actuation of the robot hand or by another mechanism cooperating with the robot, the bolt and nut would be rotated, relative to each other, in the loosening direction. During the rotation, strain gauges in the robot hand would

measure contact forces that could be resolved into the axial contact force between the bolt and nut. The axial-force signal would be processed by the robot control system to determine the degree of bolt/nut misalignment (if any) and thus to determine any needed corrections to the position and orientation of the robot hand.

In experiments to test this concept, a robot hand held a 1/2-in. (12.7-mm)-diameter bolt against a nut that was rotated counterclockwise with a period of about 18 seconds. The left part of the figure shows an example of the axial force versus time in an experiment in which the angle between the bolt and nut axes was ≤1°. The initial rise in force of 1.3 lb (≈5.8 N) was caused by a command from the robot control system to press the bolt into the nut with this amount of force. (This level of preload was essential for reducing the effect of strain-gauge noise.) At approximately 5 seconds, the counterclockwise motion started. At approximately 21 seconds, there was a 0.5-lb (2.2-N) dip in axial force (a click), indicative of proper alignment of the nut and bolt of threads. At this point, the robot control system sensed the change in the axial force and the rate of change of axial force, and responded by generating a command to reverse the rotation in order to tighten the

bolt and nut. Thereafter, the axial force decreased as the engagement of the nut and bolt relieved some of the preload.

The right part of the figure depicts the axial force versus time in an experiment that was similar except that the angle between the bolt and nut axes was between 4 and 6° (close to the cross-threading angle for the particular bolt and nut). The initial rise in the axial force was similar to the one described above, but the subsequent clicks were smaller. The force and the rate of change of force did not change sufficiently for the robot control system to recognize "good" alignment; therefore, the system did not command a reversal of rotation from counterclockwise to clockwise. However, the axial-force signal included a periodic feature that indicated the instant when the threads could mate if they had been better aligned. In principle, the robot control system could be modified to recognize this feature and to command the fingers of the robot hand to tilt the bolt as a function of an axial-force gradient until alignment was obtained.

This work was done by Myron A. Diftler and Michael L. Ross of Lockheed Martin for **Johnson Space Center**. *MSC-22837*

38

Mathematics and Information Sciences

40

Software for Setting Up Equipment for Testing Rocket Engines

Tedious manual test procedures are replaced by programmed, automated procedures.

Stennis Space Center,
Mississippi

A computer program has been developed to shorten the time needed to set up electronic instrumentation for a hot-fire test of a rocket engine. The instrumentation in question is a modular, partly computer-controlled apparatus, the modules of which contain amplifiers and other signal-conditioning circuits. The apparatus processes signals from strain gauges and other sensors.

Before this program was developed, the modules could be set up only through a controller front panel. Signals from external sources were introduced by unpatching input terminals and applying the signals to amplifiers. The strain-gauge modules are programmed digitally by use of bytes called "option bytes." Before the program was developed, the values of option bytes needed to balance strain-gauge bridge-circuit readouts were found by trial and error. In the case of a thermocouple signal conditioner, it was necessary to disconnect cables to read the true output voltage. For these and other reasons, the time needed to set up the instrumentation for each test was too long.

The program can be used to set up every module needed for a test. Both the amplifier and the remaining signal-conditioning circuitry in each module can be adjusted by use of this software. Each module can be programmed for any desired gain setting and calibration step. It is no longer necessary to resort to trial and error to balance strain-gauge bridge circuits (see figure). Programmable strain-gauge-balance reports and system-status reports can be generated to reduce setup time. The program can display real-time data, both numerically

The **Option Byte Calculation** subprogram generates this display. This subprogram calculates the value of the byte needed to balance a bridge circuit in a strain-gauge module.

and graphically, and can display the internal memory of the test apparatus; these capabilities can be utilized to diagnose any suspected defect in a measurement or in the entire testing system.

A unique feature of this program is that setup information is sent from the computer that runs the program, via a serial communication port, to a hand-held "dumb" terminal that includes a small display screen and a keypad, which resembles that of a pocket electronic calculator. This feature makes it possible to perform the test setup from either the computer or the dumb terminal. The dumb terminal displays as many as four

lines of information from a test-setup-window display on the computer terminal. Each key on the keypad corresponds to a button in the test-setup window. A technician can easily move to and adjust a module while viewing the display on the dumb terminal.

This work was done by Michael W. Burge of Rocketdyne Division of Rockwell for **Stennis Space Center**.

Inquiries concerning rights for the commercial use of this invention should be addressed to the Technology Transfer Office, Stennis Space Center, Attn: John Bailey (228) 688-1660. Refer to SSC-00093.

NSUTCQ: an Alternative Image-Compression Algorithm

This algorithm could be especially useful for remote viewing of medical images.

John H. Glenn Research Center,
Cleveland, Ohio

No-shift universal trellis-coded quantization (NSUTCQ) is an image-data-compression/decompression algorithm designed to be especially useful in telemedicine. Like some other image-compression/decompression algorithms, this one provides both (1) lossy compression/decompression for transmission of most of the information in an image subject to competing requirements to limit transmission time, transmis-

sion bandwidth, and image distortion and (2) lossless (or constrained-loss) compression/decompression for transmitting the residual information (the remainder of the information necessary for reconstruction in full detail) about regions of interest (ROIs) within images. Thus, in telemedicine, a diagnostician could preliminarily view less-detailed versions of images, then select ROIs that appear to be significant and

request reconstruction of the fully detailed versions of the ROIs.

The NSUTCQ algorithm is a modified version of a previously developed lossy compression/decompression algorithm called "adaptive wavelet/universal trellis-coded quantization" ("wavelet/UTCQ" for short). The wavelet/UTCQ algorithm begins with the use of a wavelet decomposition to transform gray-scale images into wavelet coefficients.

This X-Ray Image of a Hand was digitized and its data compressed by a factor of 62 before reconstruction. The two regions of interest delineated by white rectangles were compressed by the residual-encoding scheme and therefore exhibit sharper detail than do surrounding areas.

arithmetically encoded in an eight-state trellis-coded quantization (TCQ) scheme.

The NSUTCQ algorithm differs from the UTCQ algorithm in two major respects:

1. Changes in the quantizer, involving codebook structures, probability models, and other mathematical considerations too complex to be described here, reduce the sizes of the quantization steps. Absolute errors should therefore be smaller.

2. A subalgorithm that involves a defined error tolerance and binning with adaptive arithmetic encoding of residual values for ROIs has been added. The figure is an example of a reconstructed image with two residual-encoded ROIs.

The UTCQ and the NSUTCQ algorithms both have their places in an image-compression/decompression scheme in that their capabilities are complementary. The NSUTCQ performs better at high bit rates. An examination of bit-rate allocations made by an experimental encoder that implements both algorithms revealed that low-frequency subbands were compressed at high bit rates while high-frequency subbands were compressed at low bit rates. Therefore, it makes sense to use both quantizers, choosing the one that best suits the wavelet subband being quantized.

The wavelet decomposition can be followed by an adaptive subblock classification to improve coder performance. Next, the wavelet coefficients in the subblock are quantized. The quantization subalgorithm can be characterized as a highly structured vector quantizer or as a scalar quantizer with memory. The quantizer processes the wavelet coefficients into quantization indices. The quantization process is lossy; that is, it introduces distortions into the wavelet coefficients. The goal in designing a good quantizer is to ensure that the distortions do not seriously degrade the reconstructed imagery. In the wavelet/UTCQ algorithm, the quantization indices are adaptively

Software for Scanning, Storing, and Retrieving Images

An application program for scanning and storage of images and for retrieval of the images via the World Wide Web has been written in the Java programming language to be portable to any computer and operating system that support the Java Virtual Machine 1.02. The program can be run on one computer or spread across three computers: a client, a server, and a third computer that stores the image data base. The data from scanned images are stored in the TIFF Group IV format and can be retrieved in that format or converted to portable document format (PDF) for viewing through an Applet interface; the conversion to PDF is done,

on demand, by a portion of the software that resides on the server. Although the program stores files in the TIFF format, it also supports any other format, and image data stored in any format are retrieved in their native form. Once an image is scanned into the data base, it is immediately available for retrieval. The program includes callable interfaces with other data bases and application programs. It also provides capabilities for administration of the image-storage and -retrieval system.

Software for Environmental Monitoring in a Large Facility

Four computer programs enable the nearly real-time distribution, analysis, and display of data on temperature, relative humidity, and particle fallout measured by sensors in the Orbiter Processing Facility (OPF) and the Launch Pad Payload Changeout Room (PCR) at Kennedy Space Center. The previous environmental-monitoring software distributed data only once per hour; did not provide for rapid, automated analysis; and was not flexible enough to accommodate new sensors. Under the present software,

readings are taken from the sensors every 2 minutes and transmitted over local-area networks to a server computer. Any computer on the network can display the data as both numerical values and colors (green, yellow, or red for within, almost out of, or out of specification, respectively). Out-of-specification data is also signaled by audible beeps. Optionally, daily graphs of data can be displayed. The programs, written with LabVIEW software, are modular and can be modified easily to accommodate new sensors, change the sam-

pling interval, enable or disable audible alarms, or rescale graphs.

This work was done by Paul Berry and Chuck Hamden of United Space Alliance for **Kennedy Space Center**. *For further information, see TSP's [page 1].*

Inquiries concerning rights for the commercial use of this invention should be addressed to the Technology Programs and Commercialization Office, Kennedy Space Center, (407) 867-6373. Refer to KSC-12008.

Books and Reports

Quick Guide to MSAT

A report presents additional information on the Mechanical System Design/Analysis Tool (MSAT) computer program, which was reported in "Program for Designing a Mechanical System" (LEW-16710) *NASA Tech Briefs*, Vol. 23, No. 9 (September 1999), page 32. To recapitulate: MSAT is a user-friendly, multidisciplinary software system that facilitates and accelerates the synthesis and analysis of designs of mechanical systems. MSAT features a modular architecture that organizes design-analysis tasks around object-oriented representations of (1) components of an aircraft engine or other system that one seeks to design, (2) analysis programs, and (3) data-transfer links among the components and analysis programs. The report includes an introduction that briefly describes MSAT and some actual and potential applications. The introduction is followed by a concise user's guide that provides a further description of MSAT, with instructions on how to run MSAT and an example of the development of an MSAT software module for a specific application.

This work was done by HuaHua Lee, Mark Kolb, and Jack Madelone of General Electric Co. for **Glenn Research**

Center. *To obtain a copy of the report, "Mechanical System Analysis/Design Tool (MSAT) Quick Guide," see TSP's [page 1].* LEW-16888

Time-Parallel Solutions of Linear PDEs on a Supercomputer

The highly decoupled structures of time-parallel algorithms make for efficient implementation on supercomputers.

A paper describes the mathematical basis and some applications of a class of massively parallel algorithms for finite-difference numerical solution of some time-dependent partial differential equations (PDEs) on massively parallel supercomputers. In a radical departure from the traditional spatially parallel but temporally sequential approach to solution of finite-difference equations, the algorithms described in the paper are fully parallelized in time as well as in space; this is achieved via a set of transformations based on eigenvalue/eigenvector decompositions of matrices obtained in discretizing the PDEs. The resulting time-

parallel algorithms exhibit highly decoupled structures, and can therefore be efficiently implemented on emerging, massively parallel, high-performance supercomputers. The present paper illustrates the power of time-parallel algorithms for solving the equation for conduction of heat in two dimensions: in a proof-of-concept demonstration, a time-parallel algorithm was implemented in a FORTRAN program on an Intel Touchstone Delta supercomputer, using various numbers of processors from 1 to 120 and square computational meshes of various sizes from 15 to 127 lattice points per side. The speedup achieved by the time-parallel algorithm over the best serial algorithm was found to be approximately proportional to the number of processors when 120 processors were used, even on the smallest grid; the results also suggest that superlinear speedups are achievable on larger grids.

This work was done by Nikzad Toomarian, Amir Fijany, and Jacob Barhen of Caltech for **NASA's Jet Propulsion Laboratory**. *To obtain a copy of the report, "Time Parallel Solutions of Linear Partial Differential Equations on the Intel Touchstone Delta Supercomputer," see TSP's [page 1].* NPO-19385

END

02-18-00